

See discussions, stats, and author profiles for this publication at:
<https://www.researchgate.net/publication/263860912>

The origins of the brain's endogenous electromagnetic field and its relationship to provision of consciousness

Article *in* Journal of Integrative Neuroscience · April 2014

DOI: 10.1142/S0219635214400056 · Source: PubMed

CITATIONS

4

READS

120

1 author:



Colin Hales

Ytek P/L

8 PUBLICATIONS 14 CITATIONS

SEE PROFILE

Some of the authors of this publication are also working on these related projects:



Private [View project](#)

The origins of the brain's endogenous electromagnetic field and its relationship to provision of consciousness

C. G. Hales

*Neuroengineering Laboratory
Department of Electrical and Electronic Engineering
University of Melbourne, Australia
cghales@unimelb.edu.au*

[Received 14 April 2014; Accepted 28 April 2014; Published 24 June 2014]

As a potential source of consciousness, the brain's endogenous electromagnetic (EM) field has much to commend it. Difficulties connecting EM phenomena and consciousness have been exacerbated by the lack of a specific conclusive biophysically realistic mechanism originating the EM field, its form and dynamics. This work explores a potential mechanism: the spatial and temporal coherent action of transmembrane ion channel currents which simultaneously produce electric and magnetic fields that dominate all other field sources. Ion channels, as tiny current filaments, express, at a distance, the electric and magnetic fields akin to those of a short (transmembrane) copper wire. Following assembly of appropriate formalisms from EM field theory, the paper computationally explores the scalar electric potential produced by the current filaments responsible for an action potential (AP) in a realistic hippocampus CA1 pyramidal neuron. It reveals that AP signaling can impress a highly structured, focused and directed "sweeping-lighthouse beam" that "illuminates" neighbors at mm scales. Ion channel currents thereby provide a possible explanation for both EEG/MEG origins and recently confirmed functional EM coupling effects. Finally, a physically plausible EM field decomposition is posited. It reveals objective and subjective perspectives intrinsic to the membrane-centric field dynamics. Perceptual "fields" can be seen to operate as the collective action of virtual EM-boson composites (called qualeons) visible only by "being" the fields, yet objectively appear as the familiar EM field activity. This explains the problematic evidence presentation and offers a physically plausible route to a solution to the "hard problem".

Keywords: Maxwell's equations; electromagnetic field; compartmental model; consciousness; pyramidal neuron; hard problem.

1. Introduction

The involvement of science in the study of consciousness was recently restated as follows (Barrett, 2014):

The key question in consciousness science is: "Given that consciousness (i.e., subjective experience) exists, what are the physical and biological mechanisms underlying the generation of consciousness?"

In the same paper, physicist Adam Barrett clarified a fact of brain tissue: if you were to write down a list of all the fundamental physics involved in an account of intelligence, cognition, behavior and consciousness, that list would have a length of one: the fundamental EM (bosonic) class of the standard-model of particle physics. With the Barrett perspective, it is not a matter of whether it is EM that delivers consciousness, it is a matter of which portion of the brain's EM is doing it. But standard-model fundamental EM, in its specification from the quantum level upwards, is completely mute on consciousness. Hopefully this paper will take us a little further along the road toward dealing with that paradox.

The endogenous EM field is a natural expression of myriad field sources. This multitude of nano-scale sources superpose by vector field summation. The field system has an intricate fine structure, mirroring the fine micro-structure of the tissue as a system of field sources placed in space. Relatively weak but spatially large, the totality of the field system permeates the tissue, including all intracellular and extracellular spaces. Thus expressed, it has a seamless unity and behaviors of its own, over and above any one originating source. In a very real, physical way, the brain's EM field is a single, huge, electromagnetic entity of some kind. A captive of the neural substrate and the cranium that hosts it, the endogenous EM field is a "whole", with an operational life of its own, not obviously reflected in its contributing parts. This is the endogenous EM field of the brain.

Ultimately the field system (electric and magnetic) exits the brain, permeating the intervening cranial tissue, bone and scalp. There it becomes visible in EEG (electric field) and MEG (magnetic field) measurements. If you measure ECoG on the brain surface you are measuring spatially/temporally averaged potentials on the brain's surface produced by the endogenous electric field. Deep in tissue, if you measure the "local field potential" (LFP) then you are measuring a much finer-scale average potential produced by the endogenous electric field.

In connecting the endogenous EM field with consciousness, what we are saying is that some selected portions of the endogenous EM field produce consciousness: the experienced first-person perspective. The endogenous EM field is the loud "signal", arising from specific coherent atomic/molecular-level sources, that dominates the burbling incoherent field "noise" of the rest of the atomic/molecular-level EM phenomena. We cannot say which parts of the EM field are delivering consciousness until we figure out what actually delivers the EM field in the first place. What are these dominant atomic/molecular-level EM field sources? The answer to this question forms the bulk of the rest of this work.

While the earliest specific EM field theory of consciousness dates to 1942 (Köhler, 1960), discourse was essentially mute until the late 1980s arrival of the "scientific study of consciousness". A generic term for the science of consciousness is "The ABC Correlate of Consciousness". The most prominent in the science so far is ABC = "Neural Correlates of Consciousness" (NCC) (Chalmers, 2000; de Graaf *et al.*, 2012; Hohwy, 2012; Metzinger, 2000; Molyneux, 2010; Mormann & Koch, 2007; Neisser, 2012; Velmans & Schneider, 2007). A more recent popular contender is

the ABC = “Information Integration Theory” (IIT) correlate of consciousness ([Balduzzi & Tononi, 2008, 2009](#); [Barrett, 2014](#); [Tononi, 2008, 2004](#)). Another famous contender is the ABC = “Global Workspace Theory of Consciousness” (GWS) ([Baars & Franklin, 2009](#); [Baars, 1997](#); [Baars et al., 2003](#); [Shanahan & Baars, 2005](#); [Velmans & Schneider, 2007](#)).

In positing endogenous electromagnetic fields as the origins of consciousness we have ABC = “Electromagnetic Correlates of Consciousness” (EMCC). That is the sense in which EMCC are posed as an answer to the ([Barrett, 2014](#)) question that puts it in a critically superior position by virtue of all other “ABC theories of consciousness” actually being EM field theories in disguise. An early field theory contender is Benjamin Libet, who proposed a “Conscious Mental Field” that is (a) not in any category of known physical fields, such as electromagnetic, gravitational etc, (b) may be viewed as somewhat analogous to known physical fields and yet, (c) cannot be observed directly by known physical means ([Libet, 1994](#)). Karl Popper also lent support to a non-specific field theory of consciousness ([Libet, 1996](#); [Lindahl & Arhem, 1994](#); [Popper et al., 1993](#)). The EM-field proposition presented here eliminates all need to posit exotic field systems. As such, the exotic field propositions become irrelevant.

Exotic quantum mechanical effects have a long history of being posed as a solution to consciousness. The most recent and loudly touted form is “quantum computation in microtubules”, and recent empirical work suggests some evidence of quantum effects in microtubules. That evidence’s claim to be related to consciousness is, so far, lacking ([Hagan et al., 2002](#); [Hameroff, 1998, 2012](#); [Hameroff & Penrose, 2013](#)). The later EM-field proposition presented here eliminates all need to posit exotic quantum effects. The quantized (bosonic) EM field impressed on space implicitly supplies all the necessary quantum effects. Exotic quantum effects thereby become irrelevant.

The main EM field theories arose in late 1990s and early 2000s with the work of Susan Pickett (“*The Conscious EM field theory – CEMF*”) ([Pickett, 1999, 2000, 2002, 2007, 2012](#)), John-Joe McFadden (“*CEMI – Conscious Electromagnetic Information theory*”) ([McFadden, 2002a, 2002b, 2006, 2013](#)) and E. Roy John (“*The coherent EM field*” theory) ([John, 2001, 2002, 2003, 2005, 2006](#)).

This paper adds critical physical details to the body of support for all EM field theories. For example, it provides a direct basis for the “wave mechanics” of the ([McFadden, 2002](#)) treatment. It does this by (a) providing specific plausible, physical origins for both the electric *and* magnetic fields that are (b) consistent with all the empirical evidence used to support all field theory treatments to date (including a causal role) and that (c) also have a plausible mechanism underlying subjectivity.

In dealing with the “hard problem” of an experienced first-person perspective, and in particular with EM fields as its deliverer, we must recognize “*being the EM fields*” and “*scientifically observing the EM fields*” as fundamentally different perspectives. The former is a first-person perspective/consciousness (a faculty enabling scientific observation in the first place). The latter is what the fields look like when you use consciousness to scientifically observe them. Because of the fundamental categorical distinction between these two perspectives, heightened sceptical

attention to assumptions must be maintained. We cannot assume, for example, that causal relations between two points/events, intensity (field strength, or perhaps signal/noise ratio), temporal persistence (or otherwise) or spatial separation remain subject to the usual historical/cultural assumptions.

What is motivating this vigorous attention to the EM field system? One good reason is the fact that some aspect of the dynamic EM field system has finally been held accountable for causal effects in tissue. EM coupling therefore joins action potential (AP) signaling to become the second signaling system in the brain.^a The specific mechanism responsible for EM coupling is currently unknown. In any event, EM signaling must join AP signaling with its own formalism in neural modeling. Apart from its consciousness-related contribution, it is one of the goals here to lay down the groundwork needed to eventually add the appropriate EM field effects to mainstream neural models.

The dominant view throughout the twentieth century was that the EM field is epiphenomenal. That is, it had no functional/causal role in tissue, and was assumed to merely reflect activity like the sound of a heart does for heart function. This view is shown diagrammatically in Fig. 1(a). The epiphenomenal view was not universal, as

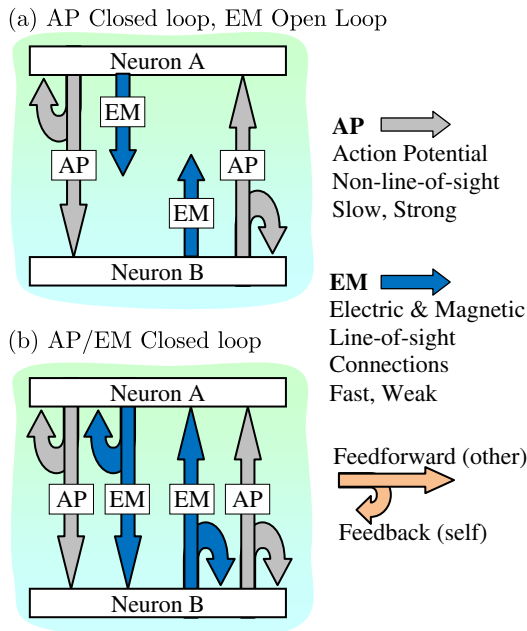


Fig. 1. (a) The traditional open-loop view holds that the fields are epiphenomenal. (b) The closed-loop view is that which accounts for recent empirical evidence in certain tissues. Based on figures in [Frohlich & McCormick \(2010\)](#).

^aSometimes called ephapsis or ephaptic coupling, although this name is likely to be ultimately regarded as a misappropriation of a term used for a medical condition.

EM field effects have been routinely reported all along, leading some researchers to expect the “closed loop” behavior of Fig. 1(b) ([Anastassiou *et al.*, 2010](#); [Aronsson & Liljenstrom, 2001](#); [Bikson *et al.*, 2004](#); [Bishop & O'Leary, 1950](#); [Faber & Korn, 1989](#); [Francis *et al.*, 2003](#); [Jefferys, 1981, 1995](#); [Jefferys & Haas, 1982](#); [McIntyre & Grill, 1999](#); [Noebels & Prince, 1978](#); [Parra & Bikson, 2004](#); [Rall & Shepherd, 1968](#); [Reato *et al.*, 2010](#); [Taylor & Dudek, 1982](#); [Terzuolo & Bullock, 1956](#)). The cultural partitioning of views, along open/closed loop EM field lines, was sufficiently unsettling that it once led to a call for resolution ([Bullock, 1997](#)). EM field feedback, despite evidence to the contrary, can still be found declared hypothetical ([Weiss & Faber, 2010](#)).

Now, sufficiently inspired, technologically feasible and compelling empirical work supports the Fig. 1(b) closed-loop view ([Anastassiou *et al.*, 2011](#); [Frohlich & McCormick, 2010](#); [Reimann *et al.*, 2013](#)). The feedback effect can no longer be claimed epiphenomenal. It is not a matter of whether it happens. It is a matter of how the effect arises. The originating mechanism provided in this paper is consistent with the closed-loop form of Fig. 1(b), including, eventually, its quantification. The EM feedback is a result of the action of later Eqs. (11) and (14) for the dynamic electric and magnetic fields, respectively. Based on Eq. (14) it may also be possible that, at very small distances, even the tiny magnetic field can have a self-feedback causal effect. Just like wires carrying current can attract each other, ion channels firing together may be attracted to each other, moving laterally in the plane of the membrane to collocate into clumps of channels.

Not all tissue need be expected to operate as per Fig. 1(b). If function can be satisfied without EM feedback, then the anatomy and physiology of the cells may self-organize to simply not make use of it (lower cell density, for example, reduces EM coupling effects). In that case the functional equivalent of Fig. 1(a) would result. It becomes a matter of the requirements of the tissue. It is therefore an obvious expectation that tissue functional EM field effects will be found to operate on a spectrum of roles, with Figs. 1(a) and 1(b) forming the extrema of possibilities. It is hoped that the potential for a sophisticated and subtle feedback mechanism is at least in-principle demonstrated here.

2. Nervous Tissue and EM: Fundamentals

Consider Figs. 2(a) and 2(d), which depict the physical reality of cortical grey matter formed by the intimate interweaving of thousands of neurons and astrocytes, each of which has an intricate branched structure spanning hundreds/thousands of μm . Setting the intracellular molecular machinery aside, the tissue is essentially water electrolyte radically fragmented/partitioned by neuron and astrocyte cell membrane (non-conducting lipid bilayer) at the sub-micron level. The so-called “extracellular space” (ECS, shown in red in Fig. 2(a), and detailed in 2(c), is actually a nano-scale “sheet/tunnel matrix” largely 40–110 nm across (maximum) and approaching even closer when involved in a synapse ([Kinney *et al.*, 2013](#); [Mishchenko *et al.*, 2010](#)).

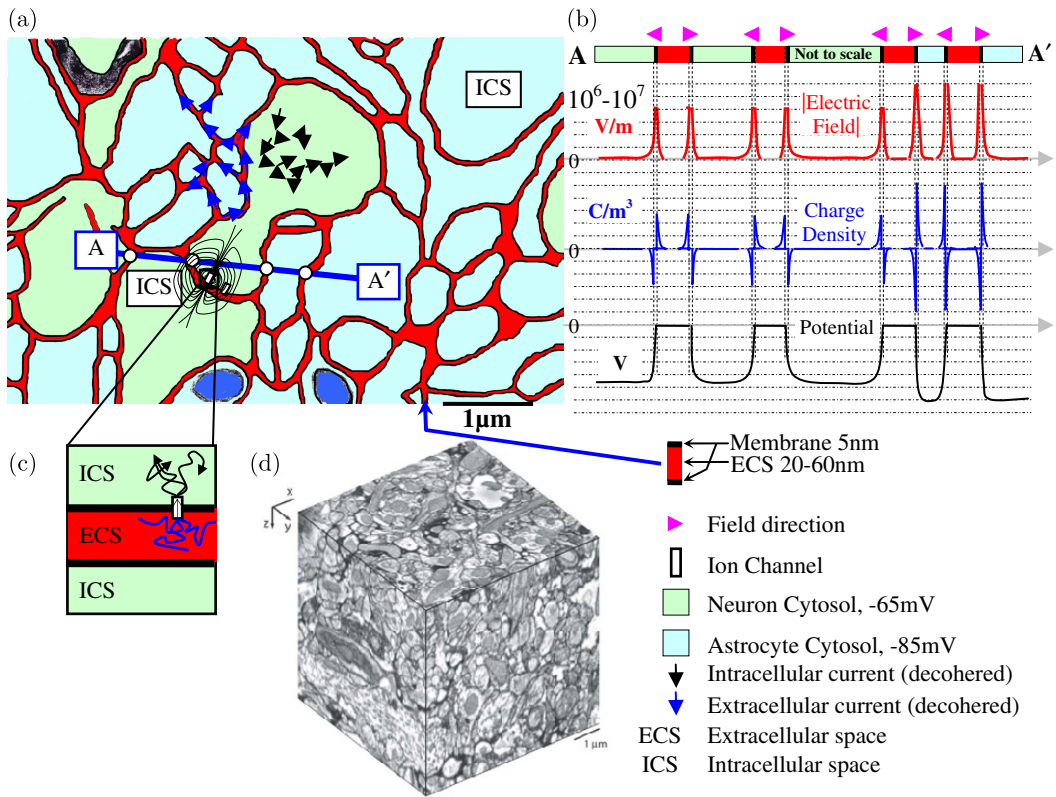


Fig. 2. (Color online) **EM field coherence origins in nervous tissue.** (a) is a notional portion of a slice through (d) that reveals EM field system origins. Transporters create tortuous folded sheet-charge transmembrane dipoles shown in (b) astride each membrane boundary (black) of the ECS fluid (red). Line A-A' shows a typical line-of-sight profile of (equilibrium/resting conditions) static charge, electric field strength and potential at each intersection with membrane (Aidley, 1998; Dayan & Abbott, 2001; Hille, 2001; Johnston & Wu, 1995). Ion channel activity in (a), highlighted in (c), produces electric and magnetic fields as described elsewhere here. The \blacktriangleright arrow heads indicate the direction of the resting electric field. Potentials are referenced to the ECS as zero volts. Blue/black arrows and (c) show the same transmembrane current decohered in the ECS and ICS. The foam structure serves to decohere overall current flow at the scale of μm and above. Not to scale. (a) based on (Nicholson & Sykova, 1998). (d) based on (Briggman & Denk, 2006).

While the ECS gap is very narrow, the ECS has a high tortuosity, leading to its volume fraction being typically cited as between 10% and 20% of cerebral volume (Bach-Y-Rita, 2001; Bignami, 1991; Geddes & Baker, 1967, p. 273; Nicholson & Phillips, 1981; Sykova, 1997, 2004; Sykova & Nicholson, 2008; Sykova *et al.*, 1999; van Harrenveld, 1968). This formidable complex is that which generates static and dynamic endogenous EM fields, and upon which the EM field impinges and, eventually, exits the scalp. Understanding the origins of the various components of the endogenous EM fields, as an expression of Figs. 2(a) and 2(d) material, is the central goal of this work. Prior to that, however, we have some fundamental physics and chemistry to assemble.

2.1. *Tissue and macroscopic vs. microscopic EM field theory*

There are two fundamental sets of Maxwell's equations: the microscopic form and the macroscopic form ([Craig & Thirunamachandran, 1984](#); [Jackson, 1999](#); [Nunez & Srinivasan, 2006](#)). These are tabulated in Appendix 1. The traditional material/constitutive/macroscopic form of Maxwell's equations (that have such things as conductivity, permittivity, permeability) has been derived from the microscopic form (in which there are no materials, just atoms/charges behaving in regular ways) ([Jackson, 1999](#), Chapter 6). Brain tissue is a non-homogenous, anisotropic, non-stationary, non-linear, far-from-equilibrium complex system detailed at the nano-scale. It does not take much analysis to see that the conditions under which Jackson validates the macroscopic form are violated by brain tissue. However, the macroscopic form has been used beneath these "Jackson" limits for so long in so many contexts, that we must suppose that by careful description of components of the tissue, and by "acting-as-if" macroscopic material EM is applicable, we can glean some understanding. That understanding, however, does not alter the fact that, ultimately, it is likely that atomic level molecular dynamics incorporating a full set of Maxwell's microscopic equations (convective/diffusion form, electric and magnetic fields and the Lorentz force) will ultimately be the only form fully revealing of tissue endogenous EM field origin and role.

2.2. *Electrolyte is not a "conductor"*

Assuming that Maxwell's macroscopic EM equations apply, the brain is not a formal conductor. The bulk of the tissue is water (insulator) with ions flowing through it. Therefore, it is actually a convector (note: convection does not mean diffusion) ([Sadiku, 2001](#), p. 163). The appropriate EM equations suited to the brain are like those of gas plasma. For decades, neuroscience practitioners have used voltage/current relations to characterize tissue as having certain conductance in certain circumstances. This usage of Ohm's law for voltage/current relations, while very useful in modeling, does not permit Ohm's Law to be used to characterize EM field expression. The tissue is fundamentally based on expression of dynamic non-zero charge density established at microscopic scales and then micro-manipulated on a microsecond timescale over huge areas/volumes, with macroscopic effects. Ohm's law is fundamentally based on zero charge density at an ultra-fine scale and cannot be used to accurately express EM fields in brain tissue ([Jackson, 1999](#), p. 706). What this means is that conductivity is fundamentally the wrong material property to use in assessing the relevant EM equations for excitable cell tissue. More fundamental forms of Maxwell's equations must be used. These are Eqs. (2) and (3) and the terms in the dotted ellipse.

When cited, however, the conductivity is quite instructive and still remains predictive of voltages and currents in typical laboratory measurements. A classic example is in ([Katz, 1966](#)), who cites ICS electrolyte conductivity at 3.3 Sm^{-1} , which contrasts with the ECS conductivity of 5 Sm^{-1} , which is very similar to the bulk

conductivity of sea water. This is to be expected. To satisfy the needs of the adjacent ICS on both sides of the ECS (tens of nm apart as per Fig. 2(c)), the ultra-fine ECS must have approximately twice the average charge density associated with a single membrane. With twice as much charge to flow for a given impressed electric field, the conductivity of the ECS is expected to be roughly double the ICS. Note that both these conductivities are more than “bulk brain tissue” conductivity, which tends toward that cited for cerebral spinal fluid: 1 Sm^{-1} (da Silva & Van Rotterdam, 2005). ECS and ICS electrolytes are very poor conductors, but considerably better than pure water ($5.5 \times 10^{-6} \text{ Sm}^{-1}$), which is a very good insulator.

2.3. *Transmembrane ion speed and conduction speed in copper conductor*

In Fig. 2(c), when electrolyte ions rapidly transit the membrane through an ion channel pore, patch clamp recording of a single open channel reveals a current of the order of 10^{-12} A (Coulombs per second) (Hille, 2001, p. 90). Given the transmembrane pore length of 5–7.5 nm, and that a Coulomb consists of roughly 6.241×10^{18} univalent charges, a patch clamp current measurement corresponds to a passage of the order of 10^6 univalent charges per second (a transit time of roughly $1 \mu\text{s}$). Assuming simple ion channel kinetics with an average “open” duration of 1 ms (a single spike), of the order of 1000 single-file charges will transit a single ion pore with an average speed of the order of cm/s.

Copper uses electrons as the charge carrier in a crystalline matrix. It is a formal conductor in the proper sense of the laws of EM (Ohm’s law predicts the fields in the material). The comparison with convective motions of large ionized atoms must be carefully made. The measured conductivity of copper at 20°C is $\sim 5.9 \times 10^7 \text{ Sm}^{-1}$. When you work out typical electron drift velocities in copper at physiologically realistic temperatures you discover it to be of the order $\ll \text{mm/s}$ to cm/sec with typical voltages and material geometries. This means that although the ion channel pore is a charge transport mechanism totally unlike copper, that the charge transit speeds of an ion channel pore are comparable to that of copper. This can only be attributed to the details of the quantum effects encountered between the pore walls and the ion during its highly constrained passage through the pore. The fact that the mass of the ion is millions of millions of times more than that of an electron attests to the highly energetic drive forces at work in the pore that accelerate it to a terminal drift velocity akin to copper.

2.4. *ECS/ICS ion transport through water*

Here we look at Fig. 2(a) ECS/ICS ion behavior (blue/black arrows respectively). Basic physical chemistry (Hille, 2001) tells us ion mobility relates to the local electric field intensity as follows:

$$v_{av} = u_s |\mathbf{E}(\mathbf{r}, t)|, \quad (1)$$

where v_{av} (ms^{-1}) is the average speed for an ion with a mobility u_s $\text{ms}^{-1}/\text{Vm}^{-1}$. Mobility captures the classic drift motion of basic EM texts on conduction (Sadiku, 2001). The ions, on average, move in the direction of \mathbf{E} . In reality the ions have a much greater total speed (many orders of magnitude), due to thermal (kinetic) energy, upon which this average motion is superimposed. This ECS/ICS random ion motion is shown (greatly exaggerated) in Fig. 2(c). For weak electrolyte solutions such as the ECS/ICS, using the mobility of K^+ of $7.62 \times 10^{-8} \text{ms}^{-1}/\text{Vm}^{-1}$ (Hille, 2001, p. 317), assuming they are released from the membrane entrapment shown in Fig. 2(b), and for a typical local electric field magnitude, $|\mathbf{E}|$, of 10Vm^{-1} applied parallel to the membranes, the speed of the K^+ ion is, from Eq. (1), $7.62 \times 10^{-8} \text{ms}^{-1}$. This means that in the period of one AP (1 ms), when the fields are active, an ECS or ICS ion will move a distance of a fraction of a nm. Field-motivated charge motion in the ECS/ICS, over timescales of importance — APs — is vanishingly small. The bulk of the motion is thermal noise. All else being equal, it would take many APs for an ion to traverse a distance comparable to the ECS width of tens of nm. Notice the huge difference in average speed between the ECS/ICS and the transmembrane pore speed (Sec. 2.3). This vast disparity is the basis for the dominance, in field expression, of transmembrane currents. Note that ion transport could, however, be greatly facilitated by pure thermal diffusion and charge concentration gradient flows (convection). These effects are expected, by this analysis, as a major mechanism behind localized ion motions around ion channels. What is important here is the contribution to *EM fields* when such motion occurs.

2.5. ECS/ICS and membrane as a dielectric

The lipid bilayer membrane dielectric constant is highly anisotropic, inhomogeneous and dependent on chemical composition and frequency. However, for typical purposes in neural modeling of EM fields, it can generally be accepted as around $\epsilon = 2.1$ (Dilger *et al.*, 1979; Huang & Levitt, 1977). The relative permittivity of water is well documented and is generally accepted as roughly $\epsilon = 80$ at physiological temperatures and signal frequencies. The lipid bilayer, as a non-conductor and dielectric, has a long history of being modeled as a capacitor. High frequency nonlinearity effects aside (Bédard & Destexhe, 2008; Poznanski & Cacha, 2012), the lipid bilayer has an effective capacitance of roughly $1 \mu\text{F}/\text{cm}^2$ or $10^{-2}\text{F}/\text{m}^2$ (Hille, 2001).

2.6. Fundamental EM equations

Setting aside brain tissue for the moment, the most general differential form of Maxwell's microscopic equations can be treated as a system of sources and converted to Eqs. (2) and (3) form that explicitly shows the origins of the field system in any configuration of atoms in space or even free space (see Appendix A for symbol definitions and units).

$$\begin{aligned}
 \mathbf{e}(\mathbf{r}, t) &= \underbrace{\frac{1}{4\pi\epsilon_0} \nabla \times \iiint_u \frac{\eta(\mathbf{r}', t)}{|\mathbf{r} - \mathbf{r}'|} d^3r'}_{\text{Electrostatic}} + \underbrace{\frac{1}{4\pi} \nabla \times \iiint_u \frac{\partial \mathbf{b}(\mathbf{r}', t)}{\partial t} \frac{1}{|\mathbf{r} - \mathbf{r}'|} d^3r'}_{\text{Conduction} \quad \text{Convection}} \quad (2) \\
 \mathbf{b}(\mathbf{r}, t) &= \underbrace{\frac{\mu_0}{4\pi} \nabla \times \iiint_u \frac{\mathbf{j}(\mathbf{r}', t)}{|\mathbf{r} - \mathbf{r}'|} d^3r'}_{\text{Magnetostatic}} + \underbrace{\frac{1}{4\pi c^2} \nabla \times \iiint_u \frac{\partial \mathbf{e}(\mathbf{r}', t)}{\partial t} \frac{1}{|\mathbf{r} - \mathbf{r}'|} d^3r'}_{\text{Radiation}} \quad (3)
 \end{aligned}$$

There is only one set of originating charges. In being positioned in space they have a charge density η that creates an *electric* field via Eq. (2) left. If these charges also move then they also create a current density \mathbf{j} that results in a magnetic field via Eq. (3) left. If the magnetic field changes rapidly then it creates an electric field via Eq. (2) right. If the electric field changes rapidly it creates a magnetic field via Eq. (3) right. In Eqs. (2) and (3) there are no materials. Adaptation of the equations to a material configuration, involves segregating charge carriers into collections of “bound” and “free” charges. These become the material. The kind of EM phenomena that apply in any given material circumstance depends on which Eqs. (2) and (3) terms apply. In addition to these is the Lorentz force, where a charge q moving with velocity \mathbf{v} within an electric field \mathbf{e} and a magnetic field \mathbf{b} will experience a force \mathbf{f} as follows:

$$\mathbf{f}(\mathbf{r}, t) = q(\mathbf{e}(\mathbf{r}, t) + \mathbf{v}(\mathbf{r}, t) \times \mathbf{b}(\mathbf{r}, t)). \quad (4)$$

Now, focusing in on the particular form used for brain tissue EM fields, the important aspects of Eqs. (2)–(4) are:

- (1) The tissue is a quasi-static convector. The applicable terms are inside the dashed oval. There may be tiny effects due to the Eq. (2) right term. However, this term is assumed zero at this stage because the rate of change of the magnetic field is too small to contribute to Eq. (2). Equation (3) right-hand term is similarly too small, and is additionally divided by a huge number, c^2 , making it a vanishing contribution to the field system. Brains do not radiate anything that is currently detectable by our instruments or that might have a functional relevance within tissue.
- (2) If you have a system of sources, say one entire neuron, N1, and its ECS fluid, somehow maintained in otherwise empty space, and if the neuron fired, it would express quasi-static fields \mathbf{e} and \mathbf{b} on otherwise empty space well away from the neuron. This is the mechanism by which EEG and MEG are evidenced in space outside the tissue.

- (3) The “EM coupling” effect of brain tissue is literally action at a distance provided by Eq. (4). If there happened to be another isolated neuron, N2, sitting in the field of neuron N1, then its fields would be modulated by the field system of N1. This is the mechanism of EM coupling. It does not need a tissue medium.
- (4) Magnetic field activity is driven by current *density*, not current (Eq. (3)). This means that magnetic fields from ICS/ECS currents (Fig. 2(a)) blue and black arrows), carrying the identical overall currents originating in transmembrane activity, yet dispersed and randomized over relatively huge volumes, will generate negligible magnetic fields.

3. The Origin of Endogenous EM Fields in Nervous Tissue

3.1. Coherence: The key to understanding tissue fields

The key to understanding the dominant mechanism responsible for the dynamic component of both the electric and magnetic fields is spatiotemporal *coherence*. Ion motion synchronized in position, direction and time produces coherent currents. The resultant field system will dominate all other charge positions/motions. It is obvious how a plaque of hundreds of physically adjacent ion channels, all conducting ions at the same time implements exactly this very coherence.

3.2. The three origins of tissue fields

Using the idea of coherence, and considering this over short and long terms, and then adding the background transmembrane static electric field system, we immediately isolate three mechanisms that can account for the entire EM field system (electric and magnetic fields) over all times and over all spatial scales. These are depicted in Fig. 3 (in order of causality) and Fig. 4 (in order of spatial scale) and are detailed later.

In Fig. 3(a) we see the background static electric field (black outlines) impressed on space by the elaborate foam structure of Fig. 2(a)/2(d). Next, in Fig. 3(b), are myriad coherent action-potential-related (including synaptic activity) ion channel currents that modulate Fig. 3(a) transmembrane field at specific locations, producing a dynamic magnetic field and creating a dynamic transmembrane electric dipole field. Next, in Fig. 3(c), we have the result of many ion channels persisting in particular places in the membrane. These result in polarized regions of adjacent ECS and ICS that have an electric field effect of their own caused by non-homogeneous ECS/ICS space-charge equilibration effects. Systems of weak diffuse evanescent monopoles are to be expected.

A different view of Fig. 3 is shown in Fig. 4 by progression over micro–meso–macro spatial scales instead of temporal scales. In Fig. 4(a) (microscopic), a small patch of neural membrane shows (yellow) the highly confined membrane-transverse *static* electric field system of Fig. 3(a). Across this is the transmembrane (ion channel) dynamic current that produces a local magnetic field and an electric dipole. Figure 4(b)

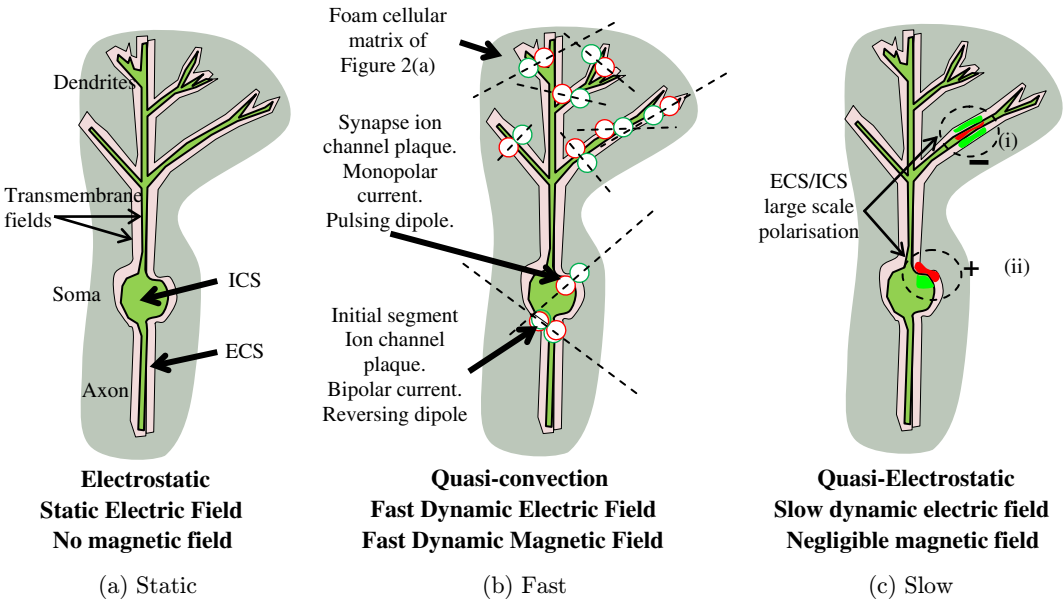


Fig. 3. (Color online) (a) The huge static electric field localized to membrane. (b) Ion channels cause pulsing/reversing dipoles that express electric and magnetic fields over large distances. (c) Persistent (b) activity causes spatially large localized polarization effects that are reset over a longer time frame. ECS (pink) is shown greatly exaggerated.

shows many of these coordinated microscopic fields dotted around the neuron. The electric and magnetic fields superpose in space. Finally, if synchronous circumstances prevail, after persistent transmembrane current at the same locations, a regional ECS/ICS polarization effect may result in an *electric field* expressed at the

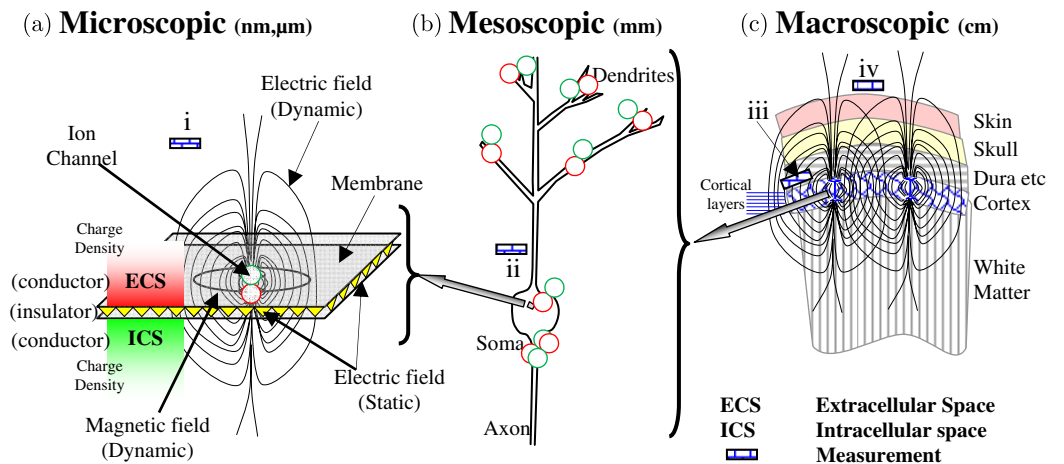


Fig. 4. Unifying the EM field system from its origins to organ level. (a) The actual origins of electric and magnetic field expression at the nm scale. Static background electric field (no ion channel activity) is modulated by dynamic electric and magnetic fields that result from ion channel activity. (b) Shows the typical depiction of the same field system (electric only) for a layer-spanning cortical neuron. (c) Is the macroscopic scale which shows large-scale charge polarization that can express electric fields. Not to scale.

mesoscopic scale. These also superpose on all the other electric fields, and become visible at the macroscopic whole organ level of Fig. 4(c).

To complete the picture, imagine active brain tissue operating normally, but in which all synapse and action-potential-related ion channels suddenly disappeared or stopped operating. All the electric and magnetic fields associated with Fig. 3(b) would vanish, taking most of the EEG and all the MEG with them. The only remnant EEG would be from Fig. 3(c) large-scale charge imbalance. As this slowly neutralizes, all residual EEG and other tissue potentials would vanish into low level tissue chemistry field noise. The message is that unless there is (a), there will be no (b). Unless there is (a) and persistent (b) there will be no (c). Note that (b) may arise in both sub-threshold and thresholded AP-related dynamics. (c) results from the sustained activity of (b).

3.3. Mechanism 1: Background static field

The underlying *static* electric field system, depicted as solid black lines in Figs. 2(a) and 3 result from charge profiles shown roughly in Fig. 2(b), which in turn leads to the electric field and scalar potential profiles shown. This is the most energetically dense field system in any tissue: the neuron and astrocyte transmembrane electrical field, which is of the order 10^6 – 10^7 V/m in the direction of ECS→ICS (Freeman, 1975; Le *et al.*, 1994; Maggio *et al.*, 2008; Peterka *et al.*, 2011; Pethig, 1986; Romijn, 2002). The static background electric field of astrocytes, caused by a membrane potential at roughly -85 mV, is about 20 mV more negative than neurons (-65 mV) (Chen & Nicholson, 2000; Kuffler & Nicholls, 1976; Magistretti *et al.*, 2002). Different ion species have different charge densities on each side of the membrane. The concentration difference for each, and in combination, is a determinant of the resting cell potential (Aidley, 1998; Dayan & Abbott, 2001; Hille, 2001; Johnston & Wu, 1995). This idea can also be extended to localised intracellular stores for specific ion species such as calcium.

The necessary charge partitioning is the result of charge transporters (pumps), shown as Fig. 5(iii), at locations that are not documented in any useful way in the literature. They act asynchronously (no ion current coherence) to restore equilibrium conditions via the conceptual reuptake cycle shown in Fig. 5. The ion transport shown as Figs. 5(ii)/5(iii) produces no functional field system (electric or magnetic) because the current density/magnitude is small, diffuse and incoherent, producing only field noise. The only field-relevant current is the dramatically cohered transmembrane current at the specific locations of ion channels shown as Fig. 5(i).

3.4. Mechanism 2: Fast, one action-potential

Figure 3(b) depicts Figs. 4(a) and 5 transmembrane ion-channel activity (singly or as a colocalized group — a plaque), powered by the static electric field system, creating a spatially large, relatively weak dynamic electric field $\mathbf{e}(\mathbf{r}, t)$ and magnetic field $\mathbf{b}(\mathbf{r}, t)$ system as outlined in Fig. 6. The magnetic field, circulating in the plane

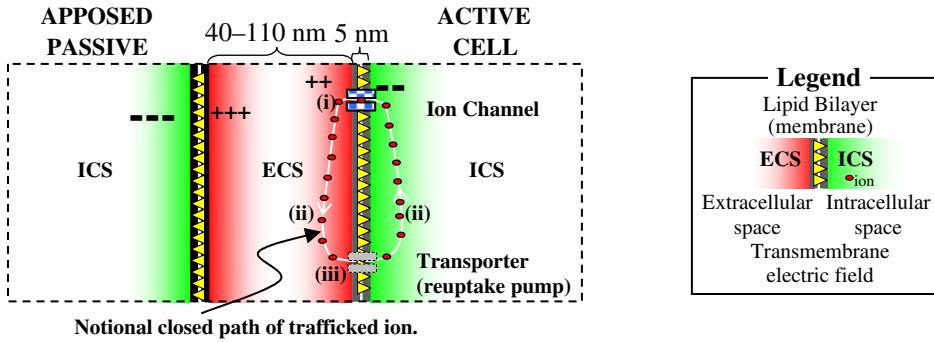


Fig. 5. Background transporters (iii) charge up the membrane, resulting in the para-membrane charge density profiles ■ and ■ that give the cells their (negative) resting potential. These act against the loss of ions due to active ion transport (i) through ion channels. Pumping (reuptake) (iii) could occur a long way from (i) the site of active trafficking. (i) FAST, COHERENT. (ii)/(iii) SLOW, INCOHERENT. (i) generates a field system that will stand out over (ii) and (iii), which are background noise.

of the membrane, lasts only as long as the ion channel current. We have already seen the dramatic difference between the transmembrane ion speeds and the ECS/ICS ion speeds. The speed of ion motion in the ECS/ICS is at least three or four orders of magnitude slower than the transmembrane ion trafficking speed (not the least of which is due to waters of hydration being dragged along with each ion (Hille, 2001)). ECS/ICS ion collision-free paths are basically limited to the size of water molecules (~0.3 nm). This is roughly 20 times smaller than the length of the (nm wide) transmembrane pore, which dramatically limits the direction of the ion trajectory.

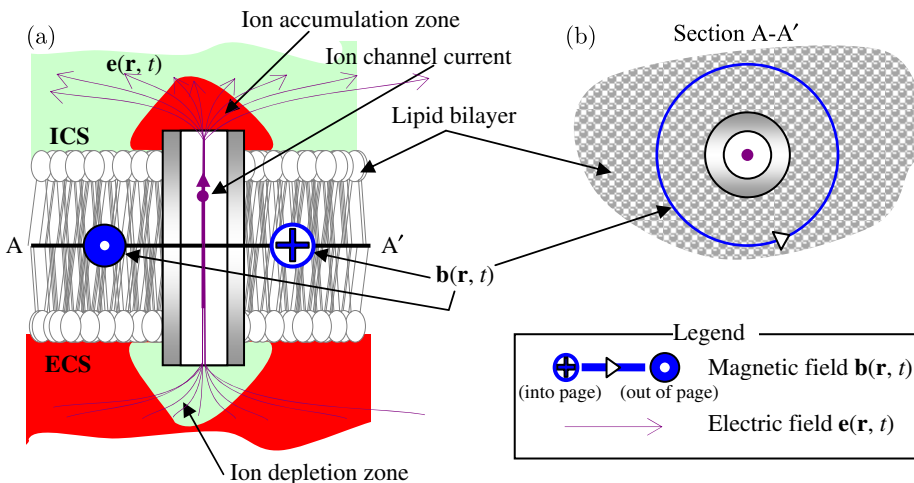


Fig. 6. The dynamic electric field, $e(\mathbf{r}, t)$, and magnetic field, $b(\mathbf{r}, t)$, characteristic of a transmembrane current filament. (a) Shows the membrane-transverse electric field arrangement. (b) Shows the magnetic field expected from the dynamics of the membrane-transverse current, shown in the plane of the membrane along section A-A'. Relatively rapid transmembrane ion traffic creates localized charge disparities in the regions proximal to the channel ends that disperse slowly because of the extremely poor charge mobility in the bulk electrolyte (ECS/ICS). The electric field lines project out into the ECS/ICS. The magnetic field strength directly follows the time course of the transmembrane current.

Ions are therefore transported across the membrane at a rate far higher than the adjacent ECS/ICS can replenish. The net result is a rapid localized depletion/accretion of charge: a local electric field dipole expressed against/astride the background transmembrane electrostatic field. This effect has been suggested in the literature previously ([Destexhe & Bedard, 2012](#)). The transmembrane charge transport dynamics are similar to that of say, a copper wire. Indeed the entire field system is simply what would be expected around a small length of wire, or within a diode, and should be unsurprising to any electrical engineer. Such dynamic electric dipoles can result from APs and/or synaptic current flows. AP currents reverse, so the dipole can reverse, reflecting the bipolar nature of the AP current. In contrast (chemical and electrical) synapses have a monopolar current, which means their dipole merely pulses.

3.4.1. *Sub-threshold behavior*

Note that sub-threshold oscillations involve transmembrane ion traffic and thereby potentially express a functionally relevant microscopic dynamic EM field contribution. Such oscillations and their fields can be expected to operate in the future mature neural modeling regimes and are outside the scope of the later computational examination of field origins. At this stage we seek merely to recognize that the proposed Fig. 3(b) mechanism also allows subthreshold oscillation as part of the “fast” field contributions, even though by definition the “AP” has not occurred yet.

3.5. *Mechanism 3: Slow, many AP*

Figure 3(c) depicts the result of an extended barrage of AP-related activity, say a whole group of collocated inhibitory or excitatory synapses. This can result in a large, more diffuse, but confined ECS/ICS charge dipole. It is basically a greatly magnified depletion/accretion zone of the kind in Fig. 6(a). Because of differing ECS/ICS charge mobilities (Sec. 2.4) and geometries, the ECS and the ICS can equilibrate back to normal charge concentrations at different rates in differing physical locations depending on the reuptake pump locations and numbers. For example, Fig. 3(c)(i) ICS is shown equalizing faster than the ECS portion, converting it from a dipole to a negative electric monopole. For the same reasons, and at some distance, monopole Fig. 3(c)(i) forms. The two pseudo-monopoles may then form a weak and fading dipole field system linking the positive and negative monopoles. This is the only way the traditional large scale electric polarization, e.g., ([da Silva & Van Rotterdam, 2005](#); [Kandel & Schwartz, 2000](#); [Nunez & Srinivasan, 2006](#); [Speckmann & Elgar, 2005](#)) can work in practice. While the localized monopoles exist, weak quasi-static electric fields form a bulk tissue regional atmosphere in which Figs. 3(a) and 3(b) field systems operate until overall neutrality is restored or reversed by ion pumps and electrolyte charge flows. Note that both Figs. 3(b) and 3(c) may have an EM-coupling functional effect on signaling. The relative contribution of each is not something examined in this paper.

4. Compartmental Models and the 3 Mechanisms

Here the three Fig. 3 fundamental mechanisms are related to the currents in traditional compartmental neural models. The microscopic current mechanisms and the traditional compartmental model are shown side by side in Fig. 7. In Fig. 7(b) the membrane is a capacitor C in parallel with a non-linear circuit element g , and its reversal potential “battery” E . One parallel branch per ion channel type. All ECS \rightleftharpoons ICS ion species (sodium, potassium, etc) and capacitive currents are covered.

A compartmental model is constructed to replicate transmembrane voltage $V(t)$ and overall currents, not the electric/magnetic fields. In using the lumped circuit element model, EM fields are abstracted away. In reality only a subset of the currents labelled 1...5 in Fig. 7(b) actually generate the coherent EM field. Components g and E are actually inside the dielectric of C . Also hidden within E current is a further division into a large number of small currents associated with ion transporters involved in the charge reuptake (notionally elsewhere on C) cycle of Fig. 5. As already discussed these currents restore the background static field across the membrane. This is how Fig. 3(a) mechanism 1 is hidden in the model within the current labeled 4 in Fig. 7.

Figure 3(b) electric and magnetic field system is created by the activity inside g and E (current labeled 3) that is actually inside C in Fig. 7(b). In contrast, the ECS current (Fig. 7 current 2) and the ICS current (Fig. 7 current 1) both produce only field noise as discussed earlier. The previously discussed dipole/monopole effects behind the Fig. 3(c) electric fields can be thought of as a result of persistent charge stored in C , captured by nonlinear effects in g that asymmetrically bleed away,

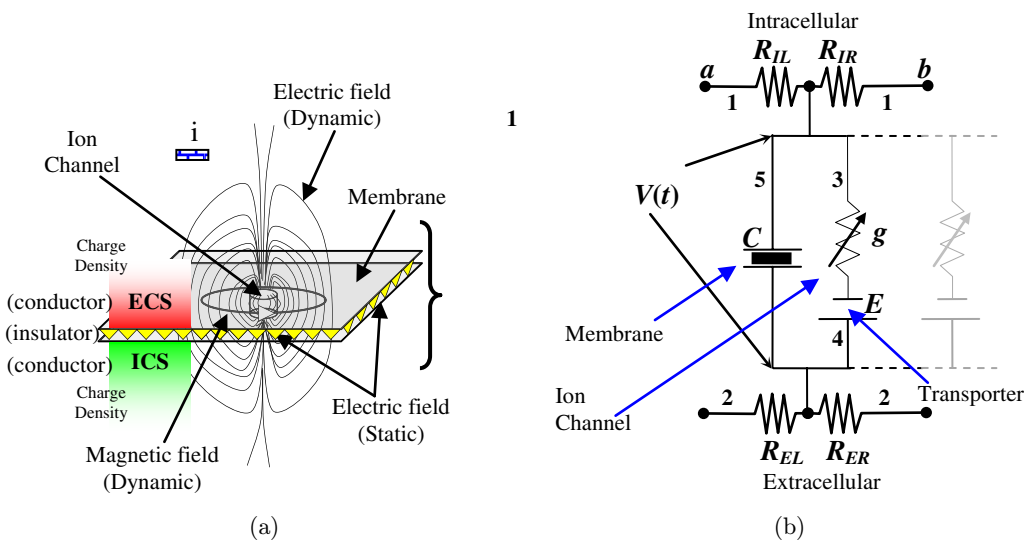


Fig. 7. The generally accepted fundamental unit of the AP signaling system in compartmental “lumped-circuit” element equivalent-circuit models.

possibly to other compartments through the resistors, thereby creating the possible monopole activity described above.

By connecting compartment to compartment (by components R_{IL} , R_{IR} , R_{EL} and R_{ER} in Fig. 7(b)) end to end, branching and terminating, complex generalized cell topologies can be modeled ([Aidley, 1998](#); [Dayan & Abbott, 2001](#); [Hille, 2001](#); [Hodgkin & Huxley, 1952a,b,c,d,e](#); [Hodgkin *et al.*, 1952](#); [Izhikevich, 2007](#); [Johnston & Wu, 1995](#)). The compartment model is quite general. In addition to AP ion channels, it allows for both electric and chemical synapses and sub-threshold oscillations, each of which produces its own distinctive field system component in space. Space is abstracted away in Fig. 7(b). In the new EM field-inclusive models that account for both EM and AP coupling, space will have to be restored because the EM field generated by one compartment impacts (line-of-sight) other compartments and alters its $V(t)$ by means not shown in Fig. 7(b).

Note that ion channels can be sparsely located in the membrane, part of a plaque in a chemical synapse (synaptic cleft plaque), part of a plaque in an electrical synapse (gap junction) or part of a plaque involved in APs such as the axon hillock/initial segment densities. They could be on dendrites, axons or soma or nodes of Ranvier (salutatory axon propagation, ringed densities separating myelinated axon segments). In each case, rapid coherent transmembrane ion transit can be held accountable for the EM field production in the manner described here.

5. A Computational Exploration of the Coherent Dipole System Created by Transmembrane Current Filaments

Exploration of the abstract mathematics of current filaments in a uniform conducting medium revealed filaments express tiny dipoles of exactly the kind in Fig. 6. To get a basic understanding of the EM field system due to the Fig. 6 transmembrane currents (Fig. 3(b) electric and magnetic fast fields system) all we need to do is drive a spatially located set of current filaments with compartmental neuron model currents. The strategy is, therefore, to:

- (a) Delete all tissue. Replace it with an infinite uniform conductance.
- (b) Use a compartmental model to generate all the necessary currents of the kind underlying Fig. 7(b).
- (c) Drive (a) with the filamentary source current(s) of (b) placed manually at known positions in space. This mimics ion channel activity. How the filamentary source is energized is irrelevant.

This simple configuration of materials and abstract current sources, appropriately driven by tissue-mimetic transmembrane currents positioned in space, must in principle produce brain-mimetic transmembrane dipole sources of the kind in Fig. 6. Of course, in reality much more complex electro-diffusion transport phenomena are at play. This gross simplification is a starting place only. Nevertheless, it will be shown to produce field systems arguably of a form similar to that we can expect in

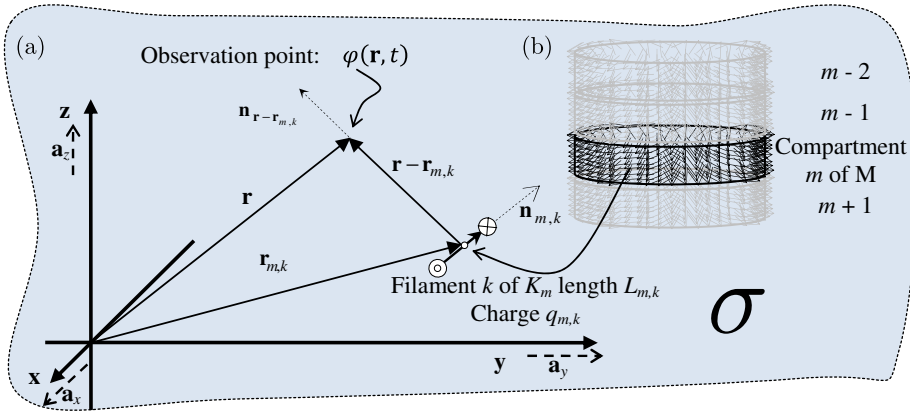


Fig. 8. A notionally infinite conductive medium of uniform conductivity σ . (a) Current $i_{m,k}(t)$ filament k within a cohort of filaments (b) K_m of compartment m of M , located at position $\mathbf{r}_{m,k}$, and of length $L_{m,k}$, contributes to the field system (in this case, scalar potential φ) at position \mathbf{r} at time t .

tissue. It can do this relatively economically. To see how to proceed consider Fig. 8 where we formalize the concept of a filamentary current in an infinite uniform conductance, yet configured in a transmembrane context.

Figure 8 shows a single current filament embedded in an infinite uniform conductivity σ . Charge $q_{m,k}$ is forced along a very short known path (mid-position $\mathbf{r}_{m,k}$, direction $\mathbf{n}_{m,k}$) by means unspecified. In doing so it constitutes a known source current $i_{m,k}(t)$ (a known current density) that may vary in time. That is, the amount of charge transiting the very short length $L_{m,k}$ of the filament k is variable over time t . To connect the individual filament to a system of filaments applicable to typical brain models, consider that filament k is merely one of a given cohort of a group of K_m filaments associated with a known neuron compartment m , which in turn is merely one of a large number, M , of such compartments located in space. One can immediately see the relationship between a physical neural membrane, the ion channels penetrating it and the typical scenario of a classic compartmental model of a neuron. Remember, however, that in Fig. 8 there is no membrane. There are only filamentary currents embedded in the positions determined as if there was a neuron membrane.

We are ultimately interested in the electric field $\mathbf{E}(\mathbf{r}, t)$ (Vm^{-1}) at a chosen observation point \mathbf{r} (meters, m) at a known time t (seconds, s). That field is the vector sum of the contributions from each of the multitude of filamentary sources in all compartments throughout a model neuron. To compute this field all we need, initially, is to get the scalar potential $\varphi(\mathbf{r}, t)$ (in Volts, V). The electric field is directly related to the potential by

$$\mathbf{E}(\mathbf{r}, t) = -\nabla\varphi(\mathbf{r}, t). \quad (5)$$

Fortunately there is a relatively well developed form of Maxwell's equations specialized to the circumstances of current sources in an infinite conductance. It is called the "volume conduction" model. It was first developed by Plonsey and colleagues in the 1960's for biological material ([Clark & Plonsey, 1966, 1968](#); [Malmivuo](#)

& Plonsey, 1995; Plonsey, 1964; Plonsey & Collin, 1961; Plonsey & Heppner, 1967; Plonsey & Fleming, 1969). A quasi-magnetostatic specialization of the fundamental macroscopic electromagnetism equations, it says that the scalar potential φ (Volts) at location \mathbf{r} and time t is

$$\varphi(\mathbf{r}, t) = \frac{1}{4\pi\sigma} \iiint_V \frac{I_V(\mathbf{r}', t)}{|\mathbf{r} - \mathbf{r}'|} d^3r', \tag{6}$$

where

$$I_V(\mathbf{r}, t) = \nabla \cdot \mathbf{J}_S(\mathbf{r}, t) \tag{7}$$

and the volume current source density, I_V (Am^{-3}), contained within volume V , has an interpretation as a “current moment per unit volume”. Mathematically the volume current density results from the behavior of a non-ohmic vector source current density \mathbf{J}_S (Am^{-2}) (Plonsey & Collin, 1961; Plonsey & Fleming, 1969). Conductivity σ is in $(\Omega\text{m})^{-1}$ and is a linear, time invariant material property that effectively renders brain material a passive, infinite, uniform continuous conducting media. The method of derivation of Eq. (6) involves an assumption that Ohm’s law applies, followed by the imposition of a known source current density that carefully violates Ohm’s law. In pure conduction, the divergence of the current density is specified as zero. The Ohm’s law violation allows the divergence to be non-zero in a localized region. At distance from the disturbance, the volume conduction formalism still applies. A further assumption is that all disturbances in the current density settle out to zero much more quickly than the spatiotemporal scales of interest. In this way, the material is essentially free of all dynamics related to the permittivity.^b This results in Eq. (6).

5.1. Customizing volume conduction to filament sources

To reach the final equation used in the computations, the Fig. 8 collection of infinitesimal current density filaments is constructed to act as sources in Eq. (7). An individual instantaneous current density filament, corresponding to notional ion channel k in compartment m , can be expressed as (Jackson, 1999; Plonsey & Fleming, 1969)

$$\mathbf{J}_{m,k}(\mathbf{r}, t) = q_{m,k} \mathbf{v}_{m,k}(t) \delta(\mathbf{r} - \mathbf{r}_{m,k}(t)), \tag{8}$$

where charge $q_{m,k}$ (Coulomb) is that of the charge species suited to a particular ion channel. The punctate nature of the ionized electrolyte atom is captured by the Dirac delta function. The instantaneous velocity $\mathbf{v}_{m,k}(t)$ (ms^{-1}) relates to the charge position $\mathbf{r}_{m,k}(t)$ as per

$$\mathbf{v}_{m,k}(t) = \frac{d\mathbf{r}_{m,k}(t)}{dt}. \tag{9}$$

^bThis does not mean that permittivity is unimportant in tissue. It means that for purposes here permittivity is regarded as unimportant. Future work can examine the impact of permittivity.

Charges travel single file (Hille, 2001) through the pore with an average velocity determined by the pore current. The direction of the average velocity is identical to the pore direction. The pore location defines the beginning of the journey through the pore, which, for a known pore current $i_{m,k}(t)$ (A), involves a known transit time for a particular pore length $L_{m,k}$.

Using an assumption that filaments have length $L_{m,k}$ that is relatively small compared to the distances of interest in the field expression, the total potential at an observed point of interest \mathbf{r} at time t is given by:

$$\varphi(\mathbf{r}, t) = \frac{-1}{4\pi\sigma} \sum_{m=1}^M \sum_{k=1}^{K_m} \left[\frac{L_{m,k} i_{m,k}(t) (\mathbf{n}_{m,k} \cdot \mathbf{n}_{m,\mathbf{r}-\mathbf{r}_{m,k}})}{|\mathbf{r} - \mathbf{r}_{m,k}|^2} \right]. \quad (10)$$

The total number of compartments is M . The total (variable) number of filaments for a particular compartment m is K_m . Vector $\mathbf{r}_{m,k}$ locates a filament in space, with a normalized direction vector $\mathbf{n}_{m,k}$. The vector $(\mathbf{r} - \mathbf{r}_{m,k})$ locates our observation point \mathbf{r} with respect to each filament in the cohort, has its own normalized direction vector as shown, and must be large compared with $L_{m,k}$. This distance limitation is consistent with the original distance limit in the volume conduction formalism of Eq. (6). Based on well-traveled compartmental neuron modeling, we know the transmembrane currents. By our choice of compartmental geometry and the positioning of current filaments in the surface of a compartment (ion channels), we can compute Eq. (10) for a collection of observation points in space. Alternatively we can use Eq. (5) on Eq. (10) and compute the electric field instead.

$$\mathbf{E}(\mathbf{r}, t) = \frac{1}{2\pi\sigma} \sum_{m=1}^M \sum_{k=1}^{K_m} \left[\frac{L_{m,k} i_{m,k}(t) (\mathbf{n}_{m,k} \cdot \mathbf{n}_{m,\mathbf{r}-\mathbf{r}_{m,k}})}{|\mathbf{r} - \mathbf{r}_{m,k}|^3} \mathbf{n}_{m,\mathbf{r}-\mathbf{r}_{m,k}} \right], \quad (11)$$

where

$$\mathbf{n}_{m,k} = \frac{(\mathbf{r} - \mathbf{r}_{m,k})}{|\mathbf{r} - \mathbf{r}_{m,k}|}. \quad (12)$$

Inserting the filamentary current Eq. (8) into fundamental Eq. (2) (left):

$$\mathbf{B}(\mathbf{r}, t) = \frac{\mu_0}{4\pi} \nabla \times \iiint_U \frac{\mathbf{J}(\mathbf{r}', t)}{|\mathbf{r} - \mathbf{r}'|} d^3 r' \quad (13)$$

Yields, using the same approximations used for the electric field,

$$\mathbf{B}(\mathbf{r}, t) = \frac{\mu_0}{4\pi} \sum_{m=1}^M \sum_{k=1}^{K_m} \left[\frac{L_{m,k} i_{m,k}(t) (\mathbf{n}_{m,k} \times (\mathbf{r} - \mathbf{r}_{m,k}))}{|\mathbf{r} - \mathbf{r}_{m,k}|^3} \right]. \quad (14)$$

We now have established a basic set of Eqs. (10), (11) and (14) describing the scalar potential, electric field and magnetic field that is expressed by the *same* cohort of current filaments, at a distance relatively large compared to the length of the

current filaments. This allows us to get a basic feel for the way we can expect the field system to operate at-distance in tissue.

5.2. Neuron model and experiment preparation

To explore the scalar potential field system, the AP-related currents in a large neuron are examined with Eq. (10). We therefore need to establish transmembrane currents and a detailed geometry. To achieve this we use a third-party compartmental model of a rat hippocampus CA1 pyramidal neuron, with a known provenance and a history of prior use. The single neuron is identified as D151 and is available via the NEURON ([Hines & Carnevale, 1997](#)) site <http://www.neuron.yale.edu>. It is called the “EAPS” package and is found under ModelDB database number 84589. EAPS stands for “Extracellular Action Potential Simulation”. It uses a different field computation method called LSA. Here, the LSA portions of the EAPS package were left unused. Neuron D151 is highly documented and has been microscopically engineered, by the EAPS originators, with the best physiological information available at the time.

The important qualification here is that there are no chemical or electrical synapses in the model. What is provided with D151 is the contribution to the field system expressed on space by the currents in the ion channels involved in a single AP. Based on the equations, significant field contributions can be expected from synaptic plaques with coherent currents. These have not been included here. Therefore the full field system expression will ultimately need all synapses and their currents, located and oriented accurately in space. Their field contribution will vectorially add to the field system produced by this work. Meanwhile we can get a basic understanding of expectations by simply allowing the AP currents to tell their part of the field-system story.

There are complications. The D151 model includes 12 different ion channel types delivering five different kinds of currents. The NEURON compartments are modeled as 1128 conical frusta (Fig. 10(b)). The underlying ion channel densities account for the best known (at the time) physiologically realistic variations throughout the D151 structure ([Gold et al., 2007](#); [Gold et al., 2006](#)). Figure 9 shows five views of neuron D151 along with its geometric (spatial) mean computed without the axon. The axon is an artificial construct with standardized dimensions and properties ([Gold et al., 2007](#); [Gold et al., 2006](#)).

To provide input data for the field computation, a single D151 AP was triggered. The EAPS package, by default, triggers an AP by slowly modulating a few Na^+ synapse conductances, thereby depolarizing the cell without introducing erroneous synapse or soma current artifacts into the EM field system. The EAPS package current report was modified to decompose the total compartment current, I_{Tot} , into I_{Na} , I_{K} , I_{cap} , I_{Ca} and I_{pas} (sodium, potassium, capacitive, calcium, passive). Additional pre-processing of current data involved their reverse-projection back onto the 1128 compartment 3D structure. Note that the D151 model current dynamics are realistic, exhibiting the usual dromic and antidromic current propagation. This

results in activity in all five classes of current. The dominant sodium, potassium and capacitative components overshadow the calcium and passive currents.

For test preparation purposes, the EAPS package was enabled, with its AP trigger delay at its default $t = 10$ ms. The delay allows the system to numerically stabilize to resting conditions. The EAPS cumulative trigger mechanism means that the AP occurs around 12 ms and continues until roughly 15 ms, during which all compartment currents go through the stereotypical variations associated with the various ion current types (see Fig. 10(a)). The balance of the 25 ms period allowed the system to settle. The recorded currents cover the period 0 ms to 25 ms (with variable time intervals of roughly 50–100 μ s). This resulted in a 159-sample time-series for all six currents for every compartment in the model. That done, the EAPS program plays no further role. The EAPS “out of the box” functionality is minimally disturbed and is left that way so that other researchers can easily replicate and expand on the results. The 3D decomposed and projected compartment transmembrane currents are displayed for compartment 1 in Fig. 10(a). The procedure that projects the D151 NEURON currents back into the original 3D geometry does not retain the ion

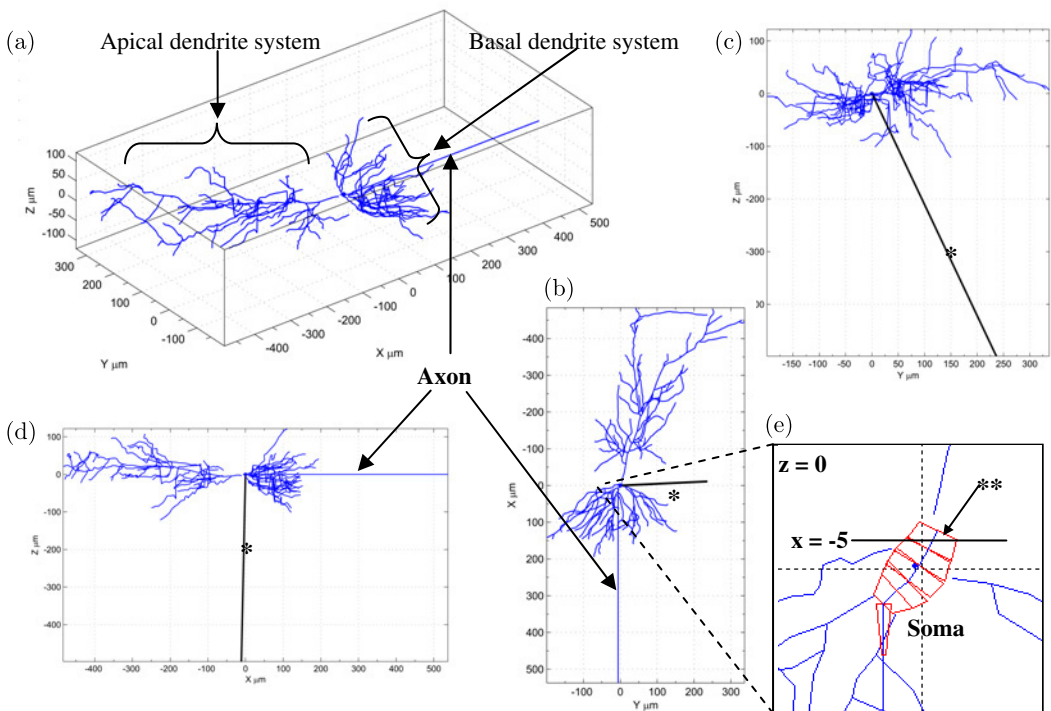


Fig. 9. Rat hippocampus CA1 neuron D151 shown in (a) isometric view, (b) XY plane viewed from $+Z$, (c) ZY plane viewed from $+X$ and (d) ZX plane viewed from the $-Y$ direction. The * indicates the single vector representing the net geometry of the apical and dendrite compartments when the compartment’s frustum centreline is treated as a vector. (e) The soma shown as fully expressed compartments in an exploded view of the origin and environs. *** frustum 1, a soma compartment which is the subject of Test 1. The soma compartment diameters average roughly 8 μ m and their height is roughly 4 μ m.

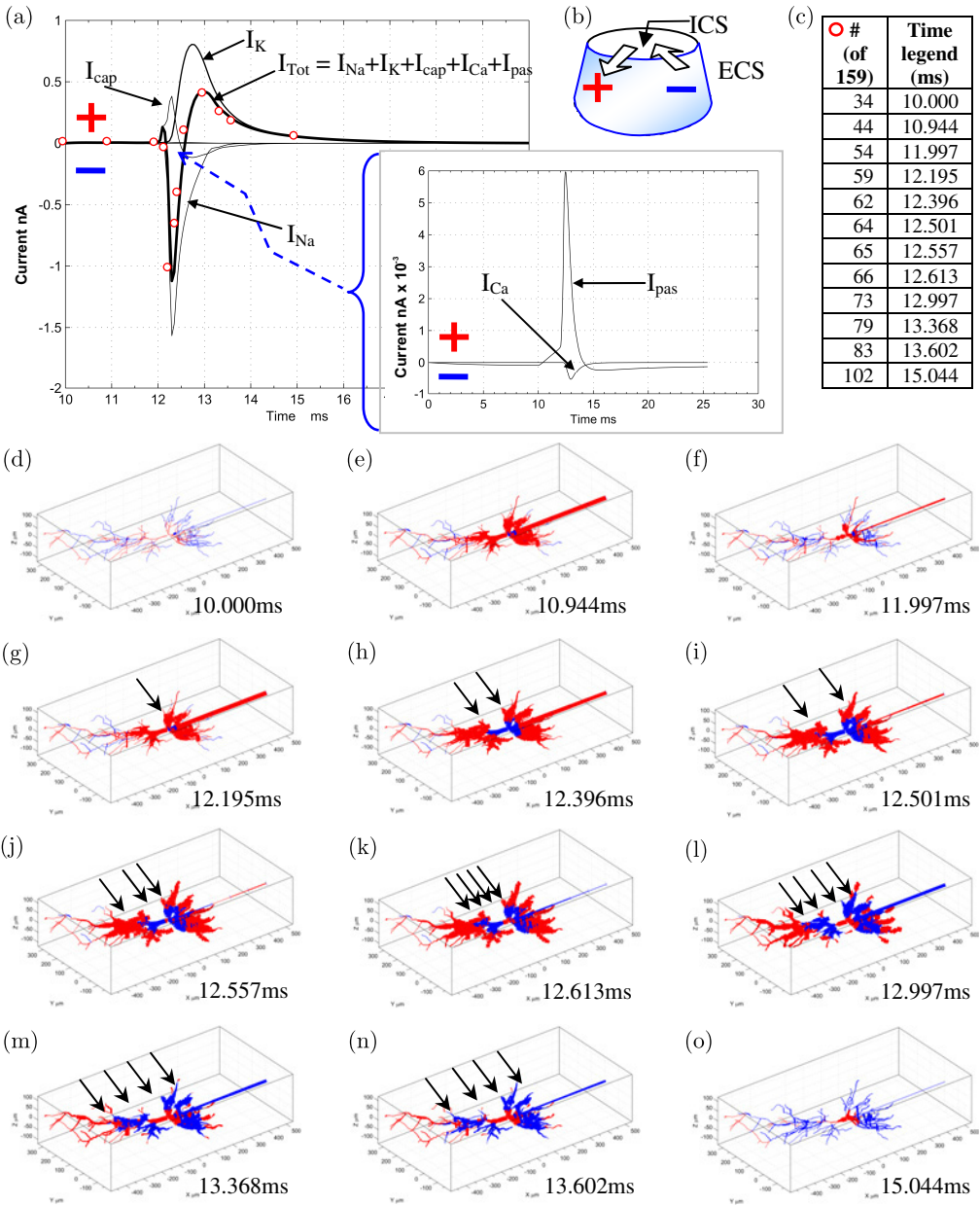


Fig. 10. Test 1. Supplementary videos S2. (a) Transmembrane currents of D151 compartment 1 of 1128. The specific compartment is marked ** in Fig. 9(e). The dark line is the total transmembrane current I_{Tot} . Currents I_{Na} , I_K , I_{cap} , are the dominant sodium, potassium and capacitive components, respectively. Currents I_{Ca} and I_{pas} , shown at an expanded scale, are the smaller calcium and passive currents. The time course proceeds according to the EAPS default setting discussed in the main text. (b) shows a typical conical frustum, indicating that the conventional positive current corresponds to outward flow of positive ions. (c) The table contains the time sample associated with the red circles in (a). The left column is the sample sequence number. The right column gives the actual time associated with that sequence number. For example, the 62nd sample occurred at time 12.396 ms. These times (and others) appear in later results and figures. (d)–(o) show the total compartmental transmembrane current propagation throughout cell D151 colour-coded as per (b). The thickness of the line is indicative of current magnitude. Arrows indicate the emergent wavefronts discussed in the text.

channel density information except insofar as the underlying NEURON simulation parameters, and hence the transmembrane currents, are affected. Overall current density variations are expected to track the ion channel density variations throughout the D151 structure.

Experiments involved the subsequent feeding of the recorded currents and geometry information into a collection of customized MATLAB programs. The most important of these custom MATLAB programs uses Eq. (10) to compute the scalar potential produced by the recorded currents when appropriately apportioned into filamentary sources positioned in space according to the geometry of the studied notional membrane compartments. In its implementation, the total transmembrane compartment current, I_{Tot} , was divided equally throughout a single cohort of current filaments allocated to the compartment. Although it was considered, it is impractical, at this stage, to individually allocate filaments to each current type and individually locate all the different filament types in different ways. There is simply no available information or obvious strategy by which this process can be administered. In view of the overall intent to merely demonstrate the basic principles of field expression by filaments, it was simply decided to use a single set of filaments that collectively conduct I_{Tot} . This choice has no effect on the basic conclusions of this work.

The filaments have a length equal to the cross-sectional width of a typical lipid bilayer penetrated by a large ion-channel protein ($L_{m,k} = 7.5$ nm filament length was used). Having allocated filaments to each compartment, each filament is then located with one end embedded in the surface of its host compartment and the other oriented orthogonally to it. What remains the same throughout this variability is the total transmembrane current. Mathematically, the NEURON model 3-D frusta are discontinuous notional constructs in a continuous conductive medium in space with Eq. (10) conductivity set at $1/3 \text{ Sm}^{-1}$ (da Silva & Van Rotterdam, 2005). This is order-of-magnitude accurate and is a determinant of field magnitude rather than the more interesting structure and dynamics. Despite this high level of material abstraction, useful realism results from the physiological accuracy of the underlying current dynamics and cell morphology.

It is not the intention of the experiments to validate the NEURON EAPS D151 behavior or accuracy, but to accept it as given for the purposes of later field computation using Eq. (10). Likewise it is not the intent of the D151 scalar potential computation to accurately predict the potential in any particular empirical context. The electric field and magnetic field are not computed, although it is a straightforward exercise and will be attended to in future work. A series of six experiments examine the spatiotemporal expression of the scalar potential field, in various contexts, during the passage of a single AP. All experiments accept, as input, the “spatialized” NEURON/EAPS current recordings described above. The overall test regime is as follows:

- Test 1: Visualize D151 transmembrane currents for interpretive purposes.
- Test 2: Examine basic scalar potential produced by regular arrays of current filaments. Uses a single D151 soma compartment.

- Test 3: Compute spatial scalar potential. Visualize slices through the 3D scalar potential field system produced by the entire D151 structure.
- Test 4: Decompose test (3) result into basal, apical and somatic contributions to see how they superpose to create the test (3) result.
- Test 5: Variability of scalar potential with filament position. Varies the filament positions to examine the scalar potential sensitivity to filament position.
- Test 6: Artificial neuron, neuron process orientation sensitivity. While keeping current filaments in the identical positions in the surface of the cell, move whole compartments in space to see the effect it has on the scalar field morphology and dynamics. Uses a particular D151 basal dendrite and the D151 soma (and the same currents each compartments normally conducts) to create a small artificial neuron for which the scalar potential is computed with the soma oriented three different ways.

5.3. Test 1: Overview of compartment currents

Figure 10 shows the results of the NEURON current computation and a spatialized, color-coded depiction of the compartment currents as expressed over time. Figure 10(a) shows the time progression of the individual and total transmembrane AP current for compartment 1 shown as ** in Fig. 9(e). The Fig. 10(a) behavior is typical of all 1128 compartments as delivered by the NEURON EAPS simulation. The dominance of the sodium and potassium currents is clear. Figure 10(b) shows the sign convention (and color code): positive current is conventionally taken to be an outward flow of positive ions. A flow of negative charge inward, *into* the ICS, is also a positive current. In Figs. 10(d)–10(o) the compartment is represented by a single line (along the axis of each frustum). Line color reflects the sign of the current. Red for positive current. Blue for negative. Line thickness indicates the magnitude of the current. Figure 10(c) shows a subset of the times at which Figs. 10(d)–10(o) is plotted. These are indicated by the small red circles in Fig. 10(a). Two supplementary videos (S1 and S2) are provided to illustrate the progression of currents throughout the neuron.

The AP current begins in the axon initial segment and immediately spreads dromically, quickly down the axon and more slowly along basal dendrites and antidromically, via the soma into the apical dendrites. The soma region cannot be seen in the stills because it is obscured. To witness the soma and initial segment, a zoomed video of the soma area is provided in supplementary S2.

Emergent behavior is evident in the progression of interfacial regions of differing total transmembrane current polarity. The sequence reveals two moving dipole fronts spreading apart in the basal and apical dendrites. These wave-fronts are arrowed in Figs. 10(d)–10(o). The triggering of the AP is signified by the early RED appearance in Figs. 10(d)–10(f). This reflects the build up of soma potential by non-specific synapse (EAPS package) manipulation and the initial positive current shown in Fig. 10(a). The change to BLUE in Figs. 10(g) and 10(h) then reflects the deep negative swing due to sodium current. The later RED in Figs. 10(j)–10(o) reflects the

return overshoot (potassium) region of the current. This activity is largest in and around the soma. Collectively expressed through the coherent action of physically adjacent branching compartments, it is easy to see the creation and progression of a pair of RED/BLUE wave-fronts of spreading virtual dipoles. While one compartment is RED, a nearby compartment is BLUE because it is in a different part of Fig. 10(a) waveform. An evanescent virtual dipole is created in space, existing only for the duration of a localized spatial current polarity disparity. It is these currents that, via Eq. (10), produce the detail of the scalar potential field of the following tests.

Finally, note what is not shown: ECS and ICS currents. These are the exact same currents shown in Fig. 10, and are represented in the *horizontal* portions of the isolated lumped-element model shown in Fig. 7(b). This current has the same current total as the *vertical* portions of Fig. 7(b). Conservation of charge and Norton's equation/Kirchoff's law means that the currents in the horizontal and vertical portions must add up to the same numerical value. The important difference is in the comparative transport dynamics and spatiotemporal coherence between the vertical and horizontal currents. It is the current *density* of each branch in Fig. 7(b) that distinguishes the vertical and horizontal branches. Despite the ECS/ICS currents being numerically identical, and reflective of the same compartmental voltage, because the current density differs, their contribution to the *field system* is completely different. Only Fig. 7(b) transmembrane (vertical) current contributes any structured field contribution. The highly confined, rapid (think gunshot) transmembrane current density represented by ion-channel-mediated charge transport constitutes a current density that dominates the field system.

As discussed above, the ECS and ICS currents are additionally decorrelated on greater spatiotemporal scales to ensure that they continue to contribute only field noise at the greater scale. It is only when the physical instantiations of the charge transport are reinstated that one can appreciate the degree to which the same current, flowing in a different way, can result in an entirely different field system in tissue. This is how the compartmental lumped-element circuit model loses contact with the field system aspect of tissue function.

5.4. Test 2: The scalar potential field of individual filaments

Prior to full scale scalar field computation, here we examine the microscopic scalar potential expressed by a regular array of individual filaments located on a single compartment. This will establish the nature of the basic building block of the scalar field system for the whole of neuron D151. To do this, neuron D151 frustum number 1 of 1128 (Fig. 9(e)**) is isolated and populated with eight rows of three filaments equally distributed radially around the frustum surface. This is depicted in Fig. 11. The dotted line is the centerline of the frustum. The dashed lines form a rough outline of frustum 1. The filament lengths are 7.5 nm and are shown greatly exaggerated in Fig. 11.

The total compartment current of Fig. 10(a) is evenly distributed throughout the 24 filaments. The potential for the lone frustum is computed in three perspectives

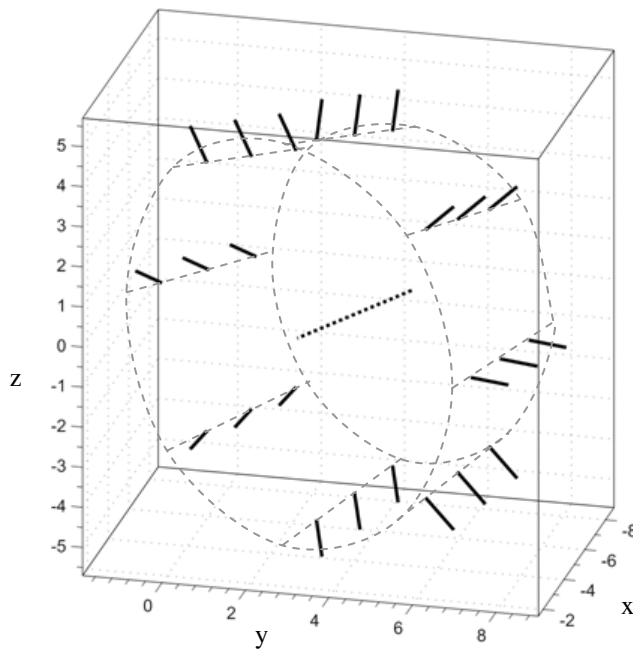


Fig. 11. Regular filament structure for Test 2. Filaments ($0.0075 \mu\text{m}$ long) are shown exaggerated, not to scale. The dotted line is the frustum centerline. The dashed line is a rough (not to scale) outline of frustum 1 marked ** in Fig. 9(e). The scale is in μm .

(XY , XZ and YZ), using Eq. (10) over the interval 11.839 ms to 15.044 ms to a spatial resolution of $0.1 \mu\text{m}$. The results are expressed in still-frame (Fig. 12) and three supplementary videos S3(XY), S4(XZ) and S5(YZ). Selected snapshot frames (from the times indicated in Fig. 10(c)) show that the computations covered a volume $25 \times 15 \times 20 \mu\text{m}$ centered on $[x = 0, y = 2.5, z = 0] \mu\text{m}$. Slices through this volume were taken as follows: XZ plane at $y = 0 \mu\text{m}$, YZ plane at $x = -5 \mu\text{m}$, XY plane at $z = 0 \mu\text{m}$. The electric field lines are orthogonal to isopotential contours (of equal color). Note that Fig. 12(b) slice intersects obliquely with compartment 1, explaining why the scalar field pattern is non-uniform across the slice.

It is easy to see the contribution of individual filaments in Fig. 12(b). A single filament would produce a pulsing/reversing dipolar plume of potential. Figure 10(a) tells us that the current at 12.195 ms is slightly negative. In the progression of Fig. 12(b), the plume increases in magnitude until it goes through the current reversal, is increasingly positive and then settles down. This is the simple reversing dipole behavior of a uniform conductor impressed by a current filament carrying Fig. 10(a) waveform. More interesting is the way adjacent coherent current filamentary dipoles superpose their scalar potential fields. Importantly, notice that the field superposition naturally preserves a zero-potential boundary located where the membrane would be in the real tissue (remember, there is no actual membrane present, only uniform conductor). Despite there being the same conductivity throughout space, the current naturally avoids the plane that would be occupied by

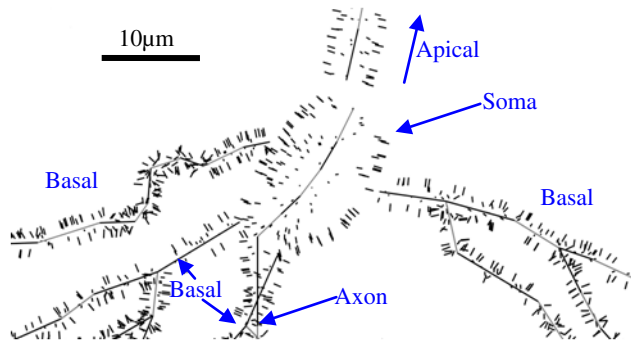


Fig. 13. Test 3. An isometric view of a subset of the random filament positions. The “soma” arrow points at the location of the same frustum #1 shown in Fig. 9(e) marked *. Filaments ($0.0075 \mu\text{m}$ long) are shown exaggerated, not to scale. The line is the frustum centerline.

resulted in 19,066 filaments. Each filament is embedded orthogonally to the frustum surface and is located by randomly determining a circumferential position and height within its host compartment. Figure 13 shows a close up view of the D151 soma region that reveals some of the filaments used in test 3.

Following the generation of the cohort of filaments positioned throughout D151 on the compartmental surfaces, test 3 computed Eq. (10) potential within planar slices through the complete field system for the entire neuron, with the currents used in the previous tests divided, on a per-compartment basis, equally amongst the filaments on each compartment. The potentials were computed on a $1.0 \mu\text{m}$ grid centered on the origin in the following specific planes and specific times: XY plane, $[(-550 \leq x \leq +550), (-550 \leq y \leq +550), (z = 0)] \mu\text{m}$, times: $11.112 \text{ ms} \leq t \leq 15.044 \text{ ms}$ and XZ plane, $[(-550 \leq x \leq +550), (-550 \leq z \leq +550), (y = 0)] \mu\text{m}$, times: $11.782 \text{ ms} \leq t \leq 14.451 \text{ ms}$. Video presentation is the best way to appreciate the result. Supplementary videos are provided; one each for the XY (S6) and XZ (S7) planes. The YZ plane was not computed due to limitations of computer time. A series of snapshots from the XY plane video are provided in Fig. 14 for the times indicated in Fig. 10(c). The XY slice at $z = 0 \mu\text{m}$ passes obliquely through the soma, which is located near the origin. Straight arrows are superimposed to indicate non-rotating fields that are shrinking/growing at a rate roughly proportional to arrow length. Curved arrows indicate rotating fields that may have an excursion in the Z -direction.

Test 3 XY and XZ videos reveal that AP-derived potentials can create a mm-scale unified, rotating lobe pattern in space. Figure 14 shows the field system spatial extent to be much larger than the basal dendrite structure. The overall scalar potential field is a rough dipole centered on and rotating around the soma/hillock/initial segment locale.

Careful observation of the video reveals that the net interaction of all the filaments produces a lobed field structure that (i) establishes itself laterally, (ii) rotates, (iii) shrinks slightly when it aligns with the axon, (iv) grows again when laterally aligned

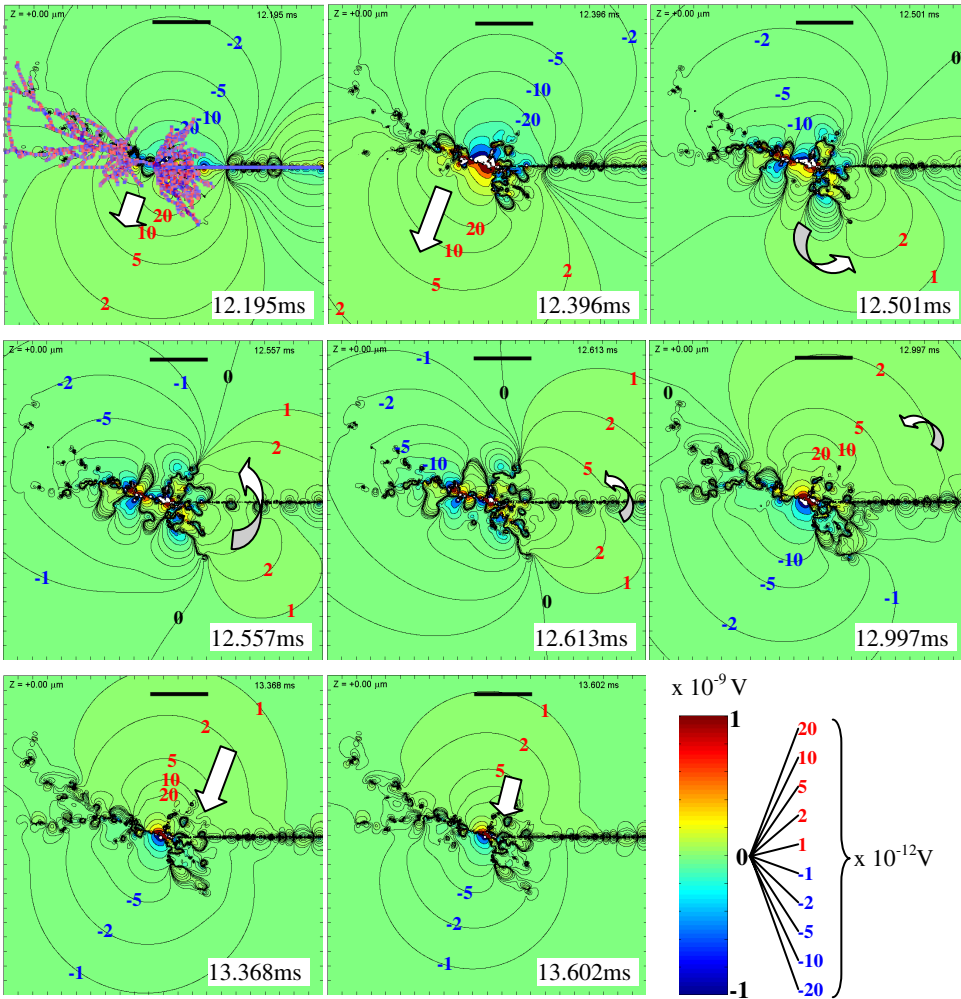


Fig. 14. Test 3. Supplementary videos S6 (XY), S7(XZ). (a) Left-right, top-bottom time progression of LFP in the plane XY at $Z = 0$ computed for the 19,066 filaments randomly positioned on neuron D151 during the single AP. The top left panel has the D151 structure superimposed. The straight arrows depict growth/shrinkage rates of a relatively stationary field pattern. The curved arrows indicate a rotating field pattern that has an excursion in the Z -direction (into/out of the page). The scale bar is $200 \mu\text{m}$.

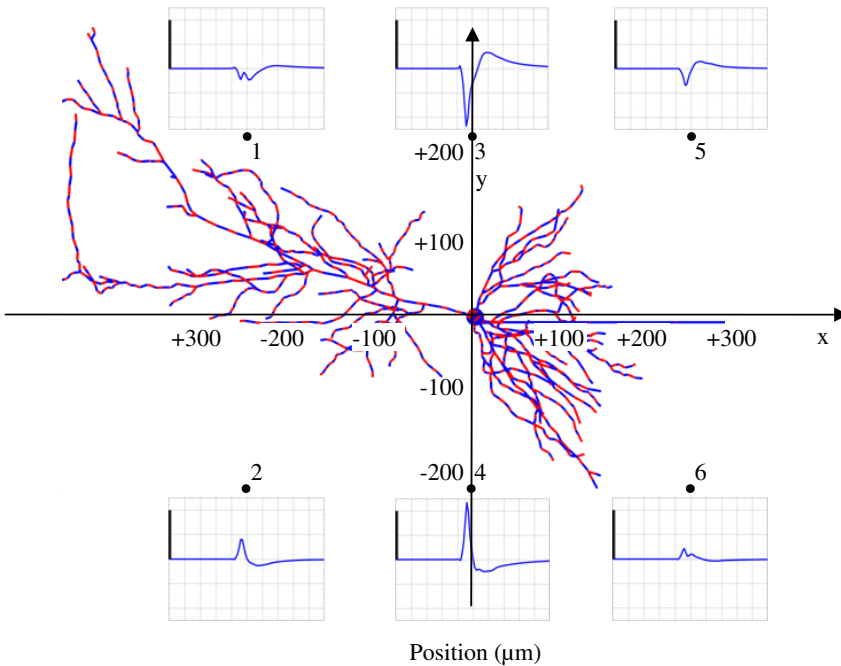
and finally (v) contracts back to the resting state. Note that the behavior is only a slice through a more detailed 3D lobe-trajectory.

Every time an AP is triggered, D151 bathes itself in a large rotating electric field. Therefore a real cell will have its own transmembrane potential modified to some extent. The field will also impact all the local neighboring neurons in the same way. The local field/charge environment around all membranes will be modified in ways that are not in the neural model that generates the original currents. The influence (already characterized above as mediated by the Lorentz force) can be viewed as a feedback mechanism. In constructing the scalar potential field system in the manner

of the NEURON EAPS model, the result can be regarded as open loop. If the field effects were built into the model then it would better be classed as closed loop, and could produce a field system differing from that shown in Fig. 14 if the closed loop modified the transmembrane currents.

Note also that in the volume depicted in the test 3 videos and images, there are 40,000–50,000 neurons all mutually interacting with each other in a line-of-sight manner. This result is consistent with an expectation that the filamentary formalisms might be responsible for EM coupling effects. The results show that the scalar potential drops off rapidly over a half mm or so, to be lost in the noise of the ECS and ICS field systems. However, proximal to the neuron out to about 200 μm, that potential, with sufficient synchrony between nearby neurons, could add up to become a functionally active potential capable of modifying firing thresholds.

Supporting this conclusion is Fig. 15, which shows that the dipole-like field behavior of Fig. 14 is consistent with the Eq. (10) expectation that the scalar potential has a time-course, at any particular point in space, which resembles the transmembrane



	x	y	z
1	-250	200	0
2	-250	-200	0
3	0	200	0
4	0	-200	0
5	250	200	0
6	250	-200	0

Fig. 15. Test 3. Scalar potential time course at specific locations 1, . . . , 6 as per the table. Distances in μm. Vertical scale bar is 0–40 pV. Horizontal extent 10 ms ≤ t ≤ 15 ms. D151 compartments are colored to reveal their collocation.

current of the dominant nearby contributing current filaments. For points near soma, the potential should resemble the AP transmembrane current time course. When dominated by synapses (in a future simulation), the potential should resemble the post-synaptic current time course. In between, the time-course should resemble a mixture of the two waveforms. The results are therefore consistent with existing empirical measurements. The six plotted potentials shown in Fig. 15 are typical of “LFP” plots seen regularly in the literature (Holt & Koch, 1999; Einevoll *et al.*, 2013), and with empirical observation (Gold *et al.*, 2009).

5.6. Test 4: Decomposition of experiment 3 results

Test 3 filaments were decomposed into three subsets: apical, basal and soma. The same slices through the scalar potential are recomputed for the three subsets of the D151 filaments. The computation is otherwise identical to test 3. The soma/axon subset (compartments 1-17) includes all filaments attached to the soma, hillock and other axon segments. Subset 18 to 507 includes all basal dendrites. Subset 508 to 1128 includes all apical dendrites. It was verified that the sum of the decomposed potentials sums to the potentials in test 3. In this test only the XY plane slices were computed for the three filament subsets. Three supplementary videos (S8-soma, S9-basal and S10-apical) are provided. Stills from these videos are included in Fig. 16.

Figure 16 reveals that the filament subsets each provide a rotating dipole. The basal and apical dipoles contra-rotate roughly in the XY plane. The third rotates orthogonally (roughly in the YZ plane) and is associated with the soma/axon complex. The decomposition indicates that temporally coherent dipole activity sums into temporally coherent dipole activity, providing a form of scale invariance. If one continued to decompose the filaments into ever smaller subsets, the result is more dipoles until finally the individual filaments are reached, all of which express fields of the kind revealed in test 2. This is an expected property of the original vector field equations, where the overall field system inherits the fundamental dipole-like character of the original active element: a current filament that originates a small scalar field dipole.

5.7. Test 5: Variability with filament position

This experiment explores how filament position affects the overall field expression by generating multiple new sets of the same filament quantities (per compartment) as test 3, but positioned differently on the D151 compartments. Ten new sets of 19,066 randomly positioned filaments were generated. Everything else is the same as test 3. The same total transmembrane current acts identically throughout the cell, again divided equally between current filaments. Because computation of the complete time series required prohibitive amounts of computer time, for each set of filaments, only the potential in the XY plane at $z = 0 \mu\text{m}$ is computed, and only for $t = 12.195 \text{ ms}$ and $t = 12.501 \text{ ms}$. This enables appraisal of (a) potential differences at specific times to be compared across filament sets and (b) the field system progression

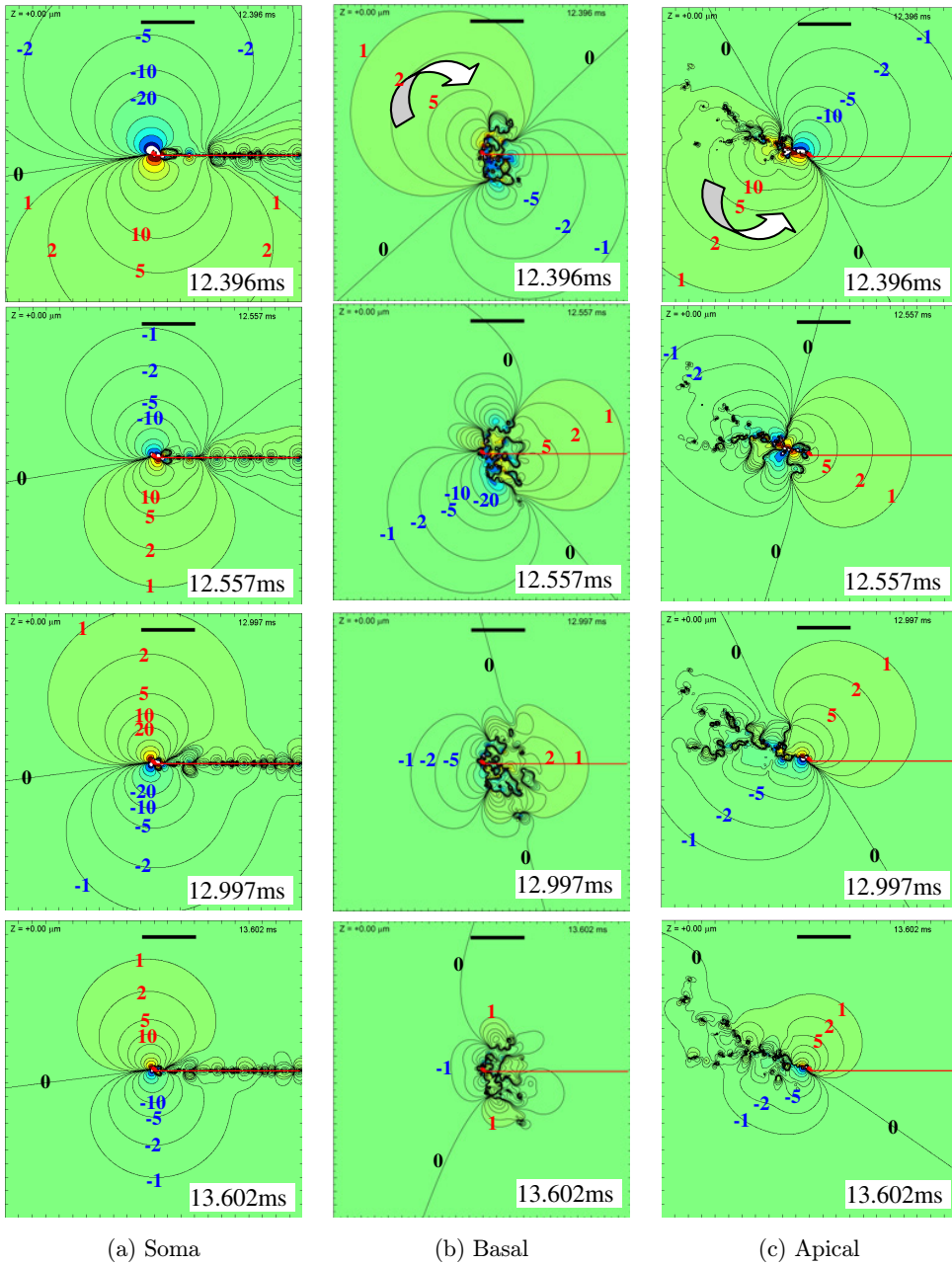


Fig. 16. Test 4. Supplementary videos S8, S9, S10. The test 3 XY field system is decomposed by region. (a) The soma/axon field system. (b) Basal dendrite field system. (c) Apical dendrite field system. The soma/axon compartment structure is superimposed in red (it lies in the XY plane). The soma/axon field system rotates in the YZ plane. The basal and apical field systems contra-rotate (directions given by the arrows) largely in the XY plane, but with trajectory including Z excursions (into and out of the page). The contour densities reflect penetrations of this XY plane at $z = 0$ by the respective processes. The scale bar is $200 \mu\text{m}$. Color scale as per Fig. 14.

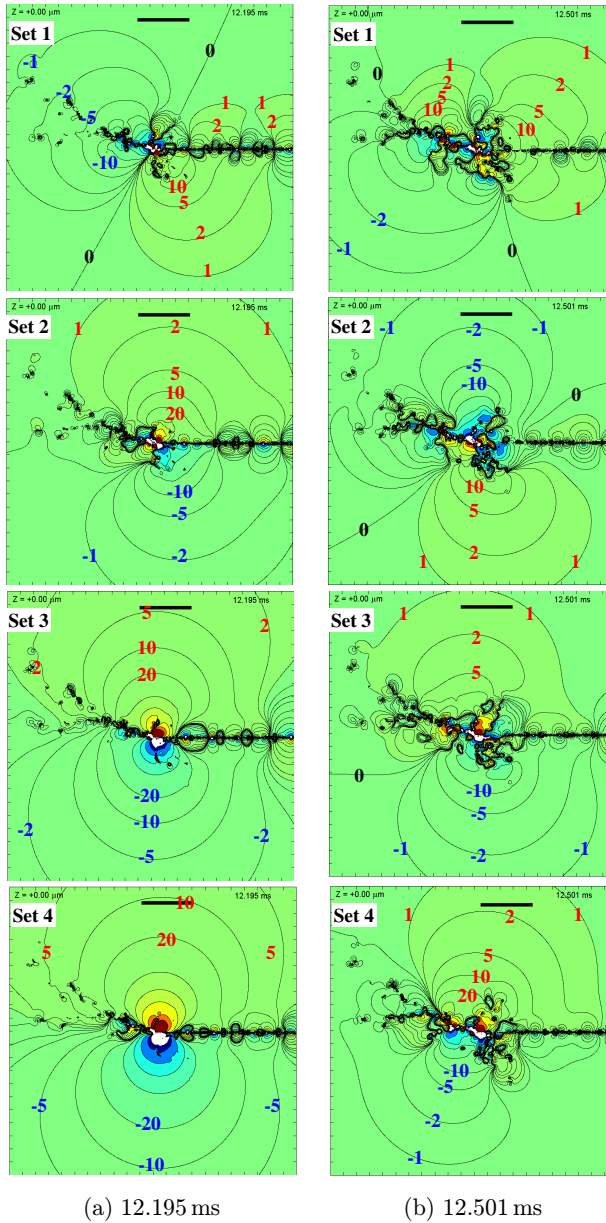


Fig. 17. Test 5. Scalar potential variability with filament position. The potential is computed at times (a) 12.195 ms and (b) 12.501 ms for 4 of 10 different sets of randomly positioned filaments. Similar variability exists for the remaining six sets, and were not included for space reasons. Test 3 planes are shown. The scale bar is $200 \mu\text{m}$. Color scale as per Fig. 14.

over time for each filament set. The results for 4 of the 10 filament sets are shown in Fig. 17.

In test 5 we discover that the macroscopic collective electric field structure and time-course is hypersensitive to the specifics of current filament distribution patterns. The result indicates that if a different filament set was used in test 3, a different set of

videos would have been generated. The significance of this result is that many different field patterns are consistent with one set of coordinated transmembrane compartmental currents.

Therefore, what has been acquired in test 3 cannot be claimed to be the final/fixed field behavior for the given cell morphology. A particular field pattern will result from a particular filament set, but only knowledge of filament details at a specific time can determine the final field pattern at that time. This supports an expectation that, in real cells, ion channel locations and densities can be expected to result in a specific field pattern. However, without detailed ion channel disposition data, the specific pattern cannot be predicted. This flexibility in the field expression can be interpreted as a novel degree of configuration freedom in neurons. The result also means that full characterization of any particular neuron cannot only include current measurements. This result suggests that to describe a neuron in a way that includes its field generation behavior, all active ion channel types and densities must be measured throughout the entire structure of the neuron.

5.8. *Test 6: Variability with cell morphology*

To test the effect of cell morphology on field expression, a simplified structure was constructed using only one D151 basal process and its soma, hillock and initial segment. An arbitrarily chosen single dendrite was used to create a small artificial neuron. To do this we aligned the chosen dendrite compartments (pulled the dendrite straight), located it in the XY plane (starting at its original start-point) and re-aligned it into the $z = 0$ plane at an angle of 45° to the x -axis. The dendrite structure was then mirrored in the YZ plane, producing a second dendrite. This resulted in a V-shaped neuron with the soma located at the apex of the V (Fig. 18(a)). Following population with a uniform filament mesh over the surface of each frustum, the structure is driven by the appropriate original D151 compartment currents. Holding the filament population size and spatial distribution constant, the resultant XY plane field system is computed for three different soma orientations covering a rotation of 180° around the V apex. A video for each soma position is provided. In this way we have controlled out all variability unrelated to pure cell morphology.

The result is that identical filament sets moved by cell morphological shift creates large changes in the field expression. Figures 18(e)–18(g) show how the field system of the two-dendrite artificial neuron varies with soma orientation as per Figs. 18(b)–18(d). Soma rotation results in the reorientation of the plane of rotation of the field pattern from the ZX plane to the XY plane and can result in a reversal of rotation direction in the XY plane. These behaviors can only result from the alteration of the relationship of the soma and its dendrites. Overall this means that fixed filament locations on a compartment can express radically different field systems dependent on the relative positioning of whole compartments. This tells us that even if ion channel types and densities were rigidly elaborated on the membrane, the field structure is still radically dependent on the cell morphology.

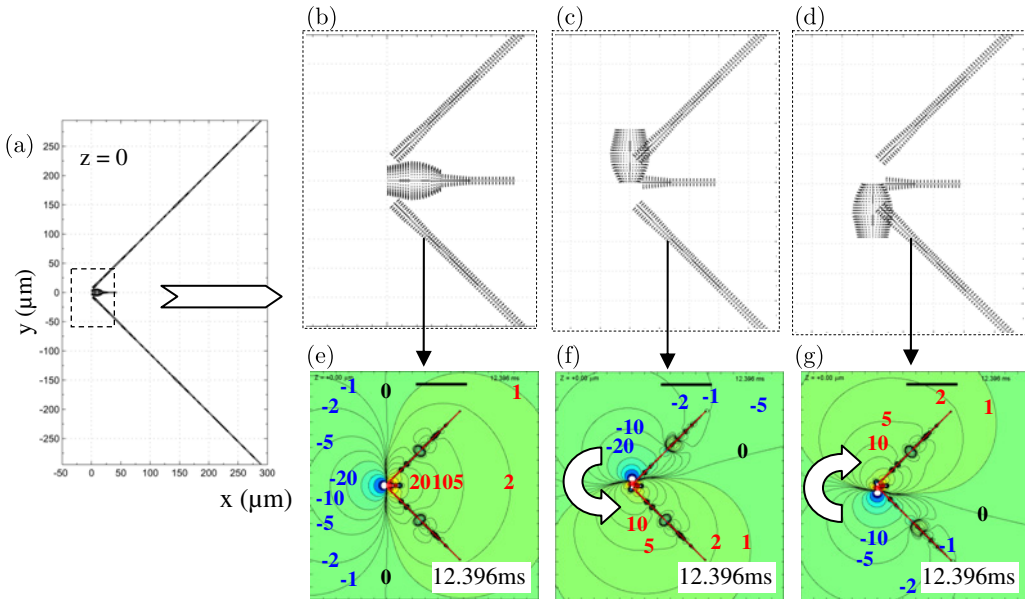


Fig. 18. Test 6. Supplementary videos S11, S12, S13 provided. Scalar potential variability with cell morphology. (a) The overall artificial neuron morphology configured as per (b), which is a close-up view that reveals the regular arrays of filaments. Cases (c) and (d) are identical in all respects to (b) except that the soma is (c) rotated 90° counterclockwise around the left end base centerline and (d) rotated 90° clockwise around the left end base centerline. (e)–(g) The scalar potential at spatial slice $z = 0$ for time $t = 12.396$ ms for (b)–(d), respectively. The arrows indicate that (f) and (g) field patterns rotate in the XY plane. No arrow is included in (e) because it rotates in the YZ plane. Scale bar is $200 \mu\text{m}$. Color scale as per Fig. 14.

5.9. Discussion

Section 5 has delivered a large computational exploration of how a neuron-shaped system of coordinated microscopic membrane-transverse current filaments expresses a scalar potential field in an infinite uniform conductance. The next task is to examine how this might inform knowledge of field origins and expression in real tissue. An earlier section established that transmembrane currents are reasonably expected to be the dominant source of dynamic field behavior. This was for reasons of basic physics: in the ECS and the ICS, the same currents are diffuse and decorrelated, lacking the current density and spatiotemporal coherence needed to produce anything more than field noise. The proposition is based on the simple idea that a transmembrane ion channel is, in effect, an intermittently conducting short length of “wire” that expresses the field system of a short length of wire. By virtue of a far higher current density, spatial coherence and temporal coherence, filamentary transmembrane current is expected to dominate the dynamic field system expressed by neurons. This idea runs counter to the view held for many decades, where ECS or ICS currents were thought to originate the endogenous field system. We now have the basic physics knowledge needed to doubt that position, especially when it so

easily accounts for both the dynamic electric and dynamic magnetic fields with the same mechanism.

But interpretive care is needed. Section 5 exploration only considered the electric field system produced by AP related ion channels. Also absent in Sec. 5 computations was the membrane itself, its para-membrane charge density profiles and its huge electric field system. This is missing because the conduction model mathematics cannot express it. Despite these limitations and a rather extreme material abstraction, the analysis supports an expectation that, in real neurons, individual ion channels, by virtue of their large numbers spread spatially over the cell surface, through their collective action and production of small, highly localized and time-sequenced pulsing/reversing dipoles, can deliver a spatially large and unified dynamic electric field and magnetic field system. Such a field system extends spatially over distances large compared to their hosting neuron and many orders of magnitude larger than the filaments themselves. The analysis revealed that the field system produced by Eq. (10) is naturally suited to the presence of a membrane, even though there was no actual membrane involved in the material abstraction. This is highly suggestive of membrane-spanning filamentary dipoles as the originator of the dynamic part of the endogenous EM field system of neurons.

The analysis revealed the field system shape and behavior to be hypersensitive to current filament spatial distribution in the membrane. In addition, even if filaments were always located in the same place on a neuron compartment, the actual relative compartment positioning (cell morphology/geometry) can radically alter the field expression. Once filament position and cell morphology is determined, the field system will be determined. Only knowledge of filament type, position in a compartment and compartment relative positions enable the determination of the final field pattern. This flexibility in the field expression can be interpreted as a novel degree of configuration freedom in neurons. In principle the same field expression can result from many different cell morphologies and filament distributions. The same cell morphology can express many different field systems. The role of this level of additional freedom in tissue development, normal function and in learning is not something that can be commented on at this stage.

Of particular interest is the possibility of highly directional and mobile sweeping "lighthouse illumination", by one cell, of thousands of nearby cells, with the lobes of the sweeping field system exhibiting focus, sweep and dwell that differ laterally and longitudinally. This is suggestive of the possibility that specific host cell morphologies and ion channel locations could be self-configured to provide some level of EM coupling directionally specialized for avoidance/preference for both host cell and/or (perhaps specially selected subsets of) thousands of its columnar and/or layer neighbors. Synchronized cell firings in a confined region may have an intricate complex interplay of EM field coupling that is unexplored at this stage.

6. The Subjective Frame of Reference and the Endogenous EM Fields

It is easy to demonstrate a reference-frame change that decomposes an objectively measurable EM field system into two systems of EM fields that account for a subjective view of the field system. If you mentally shift your perspective from that of “looking at” an EM field system to “being” the field system, then the decomposition facilitates the shift in perspective. When that is done, it becomes obvious what neural activity is responsible for the subjective view. Once formalized, in principle the reference frame shift could be computationally applied to the EM field systems delivered in the previous section. This proposal is posited merely as a way of broaching a new concept and inspiring further exploratory work.

6.1. The basis for the subjective view of EM fields

Consider Fig. 19(a) where a static field system $X(\cdot)$ interacts with an impinging field system $A(\cdot)$. During the interaction, field system $X(\cdot)$ is affected in some way as $A(\cdot)$ arrives. This is indicated in the impact zone on $X(\cdot)$. The details of the interaction are moot. Next consider Fig. 19(b) where an enhanced field system $X'(\cdot)$ is acting as if it were $X(\cdot)$ interacting with field system $A(\cdot)$. $A(\cdot)$ *does not actually exist*. $X'(\cdot)$ literally replicates all the residual phenomena that would have existed had a real $A(\cdot)$ arrived. This is denoted as a virtual field system $[A(\cdot)]$. The crucial conceptual leap is when you consider *being* $X'(\cdot)$. That is, from the perspective of being field system $X'(\cdot)$, it is “as-if” you were $X(\cdot)$ being hit by an $A(\cdot)$. If, for whatever reason, subjectively, it was “like something” to be Fig. 19(a) (for reasons unknown and unspecified), then we are forced to accept that it must, to some extent be “like that” in Fig. 19(b), without $A(\cdot)$ actually arriving. $X'(\cdot)$ delivers all the field-energetics involved in an $X(\cdot)$ colliding with an $A(\cdot)$.

This virtual interaction is the key concept in understanding the first-person perspective of an EM field system. This is meant in a literal physical sense. The physical residual EM field phenomena resulting from the collision by $A(\cdot)$ actually exists in and around $X'(\cdot)$. The collision is, to that extent, *literally reified*. Indeed we have a right to actually name a particle. If $X'(\cdot)$ is a unified EM field system maintained in space then it is, in effect, some kind of large complex composite boson or at least a bosonic entity of some kind (say a C-boson). So is $A(\cdot)$. In Fig. 19(b) we therefore have the arrival of a virtual C-boson. Indeed we can characterise the interaction as a

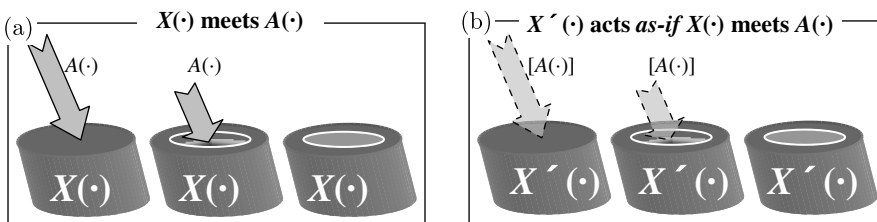


Fig. 19. Virtual EM field decomposition.

collision between a C-boson $X'(\cdot)$ and a virtual $A(\cdot)$ C-boson, $[A(\cdot)]$. In attributing the delivery of a 1st person perspective, the virtual C-boson is responsible (by means unspecified) for qualia. We can therefore call the virtual boson a *qualeon*.^c

6.2. The brain's EM field and its virtual C-boson interactions

To see how virtual EM phenomena are physically implemented in brain material (that is material behaving in the manner of the previous sections) is relatively straightforward. There is a gigantic three-dimensional foam matrix of huge static electric fields impressed on space: *the transmembrane static electric field*. This field system has the morphology of all the cell membranes in the tissue, including all neurons and astrocytes. We have depicted the reality of this “foam” previously in considerable detail. This is a huge version of $X'(\cdot)$. Embedded throughout this foam matrix, in the cell membrane, at many locations and in the many configurations discussed previously, are ion channels delivering transmembrane currents that perform major localized transformations of the electric and magnetic field systems. We humans *are* literally this structure. To be human is literally to *be* this aggregation of EM field expressions: An elaborate static background field system impressed on space, punctured dynamically by myriad small field perturbations caused by ion channels. Such perturbations may exist in the form of legions of simultaneously firing chemical or electric synapses, sub-threshold oscillations and APs. Each of these circumstances is exactly the same as Fig. 19. One such instance is further detailed in Fig. 20.

Figure 20(a) shows the objective (third person) situation. This looks like an abstraction of the simple progressively collapsing electric field on the central section of membrane (for example the “wave fronts” shown in Fig. 10). The left and right membrane sections do nothing. The situation can be seen in, say, two astrocytes astride a neuron. It could just as easily be a single neuron with different portions of its own membrane at different stages of field activity. Other neurons not currently firing would do as well as astrocytes. However it is actually implemented, Fig. 20(a) captures the objective view of a progressive field collapse traveling membrane-longitudinally.

In contrast, in Fig. 20(b) is the exact same thing viewed from the first-person perspective. In all physical respects it is identical to Fig. 20(a). The arrival of the virtual C-boson $[A(\cdot)]$ is posed as the fundamental mechanism upon which a private subjective percept is based. All that is claimed is that it is a plausible mechanism that is physically measurable and has enough flexibility to participate in a large complex of such interactions used, by the brain, to construct a “perceptual field” (like olfaction or vision). The main physical nuance is the recognition that the collapse of the longitudinal transmembrane field is identical to the transverse arrival, at a completely static membrane, of the electric field of a virtual C-boson of equal intensity and opposite direction. It is the virtual C-boson arrival that, from the perspective of $X'(\cdot)$, causes the field system collapse.

^cThis name was originated by Richard Coleman.

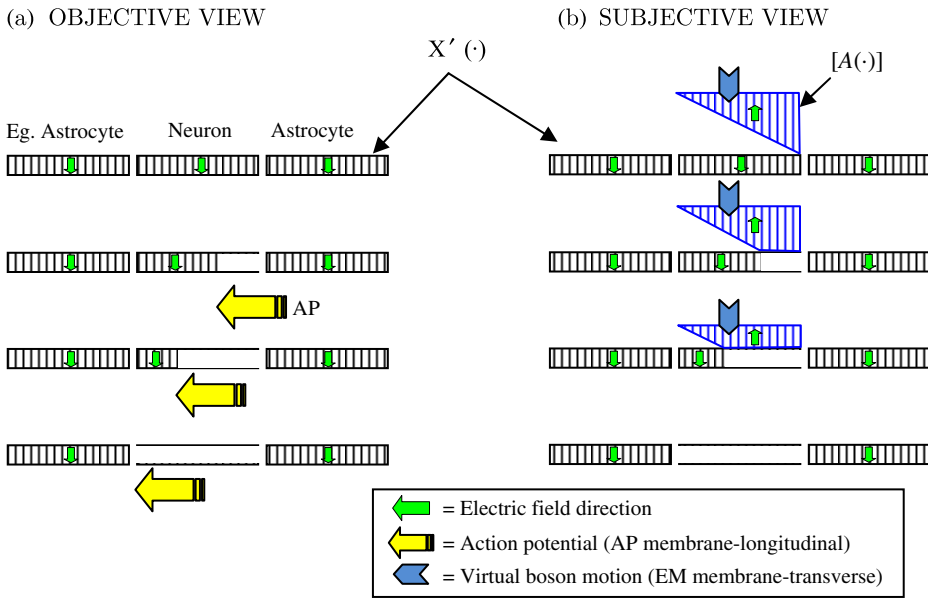


Fig. 20. (a) Objective view. The classical AP traveling wave is moving along the membrane axis. This is what the tissue looks like when measured. (b) Subjective view. From the perspective of “being” the membranes involved, (a) is identical to the membrane field remaining steady, but a transverse virtual boson arrive that literally modifies (collapses/reverses/restores) the electric field. It is “as-if” virtual boson $[A(\cdot)]$ collided with $X'(\cdot)$.

In the process of generating the field system Eq. (4) causal (Lorentz force) influences may be exerted on the surrounding tissue. If that particular activity also contributes to a first-person perspective, then we have a well understood physics mechanism for consciousness potentially being functionally active in some sense yet to be detailed. The relation between the production of the first-person perspective and the EM coupling effect is of great interest in such issues as the role of consciousness in effecting behavior and free will. In the spirit of setting aside assumptions it cannot be assumed that production of a first-person perspective via the virtual C-boson interaction, and the EM field coupling mechanism are necessarily related. The mere visibility of the virtual C-boson fields is all that is needed.

In real tissue undergoing normal realistic 3D real time neural activity involving untold numbers of interacting virtual C-bosons, extraordinarily complex “appearances” could conceivably be constructed using the neuron/astrocyte foam as a substrate “stage” upon which their arrival is orchestrated. Their collective action is, from a first-person perspective, highly spatially structured and could be set up to replicate an enormous number of qualeons directed at any representational process that could be thought of in the brain. For example, in the case of audition, we know that the transmission of sound physically involves electromagnetism in the form of phonons (already known as a kind of boson) that propagate through a medium. Collectively and when organized appropriately in space, a set of qualeons could, in principle, make a brain “act-as-if” phonons arrived, say in the planar field perturbations of a

multitude of appropriately physically organized synapses in the apical dendrites of neuron D151. The qualeons then become virtual phonons. In the case of vision, we know that sight involves the arrival of bosons called photons (light). Collectively and when organized appropriately in space, a set of qualeons could, in principle, make a brain “act-as-if” an interference pattern of photons arrived within the depths of the cortical layers involved in vision. The qualeons then become virtual photons of some kind or something appropriately similar to photons to be useful as a representation, say, some kind of hologram.

And so forth. Vision and audition are two examples that are relatively easy to imagine. What of more abstract perceptual “scenes” like emotion, touch, olfaction and so forth? It seems possible that abstract, completely naturally implausible qualeons could be created for use in such circumstances merely by positioning current filaments and compartments in space. The virtual C-bosons may be loosely related to the physical transduction of a particular sense organ, but they need not be. That being the case, it becomes feasible that we have a zoo of qualeons to identify and test for in brain tissue based on physical geometry, ion channel locations and their EM field activity. Such strange qualeons as the “touch-on”, the “sad-on”, the “orgasm-on”, the “pain-on” and so forth, seem entirely plausible as something to actively search for in tissue as EM field patterns in specific brain regions. By appropriately configuring neurons in space and then instigating their longitudinal membrane activity, in principle any spatiotemporally novel electrical/magnetic field structure could be devised that has a subjective view as a field (potentially an interference pattern) of qualeons. At the same time, all that any third-person would see when they looked at tissue is neurons arranged in space firing in the highly organized familiar ways seen for decades. This, it is posited, is the reason why the physics of consciousness has struggled for so long with its evidence-base for subjective experiences: a reference frame issue combined with naive disposal of EM effects in neural modeling activities. The mere identification of a reference frame change does not constitute an answer to *why* the subjective percept is conveyed by a virtual C-boson $[A(\cdot)]$.

7. Concluding Remarks

What has been presented here is a confluence of observations that forms a natural and obvious route toward an account of consciousness that includes the following general features:

- (I) The standard-model of particle physics tells us that fundamental physics of electromagnetism underpins all physics of the brain and its mind. Therefore, despite it being utterly mute on consciousness, the physics of electromagnetism, and the science of consciousness are somehow identities.
- (II) The endogenous EM field of the brain, as a well explored and empirically cogent originator of consciousness, gains critical priority over all other accounts of consciousness.

- (III) The recognition of the three basic mechanisms that jointly originate the entire EM field system. Transmembrane current filaments are the likely origins of both the dynamic electric *and* magnetic fields.
- (IV) The same field system automatically incorporates a causal (EM-field coupling) mechanism via the Lorentz force, thereby imbuing something delivering consciousness with a causal mechanism. This is the same causal influence recently confirmed in laboratory experiments.
- (V) The exact same field system can also be reinterpreted to be naturally decomposed into an interaction between a totally static field system and virtual EM “C-bosons”, thereby revealing a mechanism by which consciousness may be described and understood in an empirically tractable way. It does not explain why there is consciousness.

It is posited that this confluence of multiple explanatory virtues, along with compatibility with all existing empirical results, makes such an EM field theory a critically superior potential solution to the problem of a scientific account of consciousness. The real challenge is that the proposition is telling us that further progress involves some kind of formal, structured review of ourselves (scientists), by ourselves. But that is a matter for another day.

8. Supplementary Videos

Test	Video	Description
1	S1	D151 currents, isometric view, entire
1	S2	D151 currents, isometric view, soma close-up
2	S3	Compartment 1, regularly spaced filaments, XZ plane
2	S4	Compartment 1, regularly spaced filaments, YZ plane
2	S5	Compartment 1, regularly spaced filaments, XY plane
3	S6	D151, randomly placed filaments, XY plane
3	S7	D151, randomly placed filaments, XZ plane
4	S8	D151 Test 3 XY: soma only
4	S9	D151 Test 3 XY: basal only
4	S10	D151 Test 3 XY: apical only
6	S11	Artificial neuron, soma rotation 0
6	S12	Artificial neuron, soma rotation -90
6	S13	Artificial neuron, soma rotation $+90$

Appendix A

The following lists show the differential form of Maxwell’s macroscopic equations (MME) in SI units contrasted with the microscopic version (MmE) ([Jackson, 1999](#), p. 248).

Microscopic Differential MmE	Macroscopic Differential MME	Meaning
$\nabla \cdot \mathbf{e} = \frac{\eta}{\epsilon_0}$	$\nabla \cdot \mathbf{D} = \rho$	Coulomb's law: The spatial (divergence) rate of change of field is proportional to spatial charge density.
$\nabla \times \mathbf{e} + \frac{\partial \mathbf{b}}{\partial t}$	$\nabla \times \mathbf{E} + \frac{\partial \mathbf{B}}{\partial t} = 0$	Faraday's law: The spatial (curl) rate of change of electric field results in a temporal rate of change of the magnetic field.
$\nabla \cdot \mathbf{b} = 0$	$\nabla \cdot \mathbf{B} = 0$	The non-existence of magnetic monopoles: The spatial (divergence) rate of change of the magnetic field is zero.
$\nabla \times \mathbf{b} - \frac{1}{c^2} \frac{\partial \mathbf{e}}{\partial t} = \mu_0 \mathbf{j}$	$\nabla \times \mathbf{H} - \frac{\partial \mathbf{D}}{\partial t} = \mathbf{J}$	Ampere's law: The spatial (curl) rate of change of magnetic field combined with the temporal rate of change of the electric field determines the spatial current density. Maxwell added the displacement current term.
N/A	$\mathbf{D} = \epsilon_0 \mathbf{E} + \mathbf{P}$	\mathbf{P} is the polarization of the macroscopic material medium.
N/A	$\mathbf{H} = \frac{1}{\mu_0} \mathbf{B} + \mathbf{M}$	\mathbf{M} is the magnetization of the macroscopic material medium.

Notes and SI units:

- η, ρ = volume charge density (Coulomb/meter³)
- ϵ_0 = free space permittivity (Farad/meter) or (Coulomb/(volt meter))
- μ_0 = free space permeability (Henry/meter) or (Volt second/(amp meter))
- c = free space speed of light (Meter/sec)
- \mathbf{j}, \mathbf{J} = vector current density (Amp/meter²)
- \mathbf{e}, \mathbf{E} = vector electric field (Volts/ meter)
- \mathbf{b}, \mathbf{B} = vector magnetic flux (Weber/meter²) or (volt second/meter²)
- \mathbf{H} = vector magnetic field (Amp/meter)
- \mathbf{M} = vector magnetization (Amp/meter)
- \mathbf{D} = vector displacement (Coulomb/meter²)
- \mathbf{P} = vector polarization (Coulomb/meter²)

and
 $c^2 = 1/\epsilon_0\mu_0$.

Acknowledgments

Thanks to A/Prof. David Grayden and A/Prof. Harry Quiney for their support during Sec. 5 exploration. Thanks also goes to the D151 neuron data assemblers and the originators of the EAPS NEURON model, without which Sec. 5 work could not have happened. This research was supported by a Victorian Life Sciences Computation Initiative (VLSCI) grant number VR0003 on its Peak Computing Facility at the University of Melbourne, an initiative of the Victorian Government.

REFERENCES

- Aidley, D.J. (1998) *The Physiology of Excitable Cells*. New York: Cambridge University Press.
- Anastassiou, C.A., Montgomery, S.M., Barahona, M., Buzsaki, G. & Koch, C. (2010) The effect of spatially inhomogeneous extracellular electric fields on neurons. *J. Neurosci.*, **30**, 1925–1936.
- Anastassiou, C.A., Perin, R., Markram, H. & Koch, C. (2011) Ephaptic coupling of cortical neurons. *Nat. Neurosci.*, **14**, 217–223.
- Aronsson, P. & Liljenstrom, H. (2001) Effects of non-synaptic neuronal interaction in cortex on synchronization and learning. *Biosystems*, **63**, 43–56.
- Baars, B.J. (1997) *In the Theater of Consciousness: The Workspace of the Mind*. New York: Oxford University Press.
- Baars, B.J. & Franklin, S. (2009) Consciousness is computational: The LIDA model of global workspace theory. *Int. J. Mach. Conscious.*, **1**, 23–32.
- Baars, B.J., Newman, J.B. & Banks, W.P. eds. (2003) *Essential Sources in the Scientific Study of Consciousness*. Bradford.
- Bach-Y-Rita, P. (2001) Nonsynaptic diffusion neurotransmission in the brain: Functional considerations. *Neurochem. Res.*, **26**, 871–873.
- Balduzzi, D. & Tononi, G. (2008) Integrated information in discrete dynamical systems: Motivation and theoretical framework. *Plos Comput. Biol.*, **4**.
- Balduzzi, D. & Tononi, G. (2009) Qualia: The geometry of integrated information. *Plos Comput. Biol.*, **5**, 1–24.
- Barrett, A.B. (2014) An integration of integrated information theory with fundamental physics. *Front. Psychol.*, **5**.
- Bédard, C. & Destexhe, A. (2008) A modified cable formalism for modeling neuronal membranes at high frequencies. *Biophys. J.*, **94**, 1133–1143.
- Bignami, A. (1991) Glial cells in the central nervous system'. *Discuss. Neurosci.*, **8**, 1–45.
- Bikson, M., Inoue, M., Akiyama, H., Deans, J.K., Fox, J.E., Miyakawa, H. & Jefferys, J.G.R. (2004) Effects of uniform extracellular DC electric fields on excitability in rat hippocampal slices *in vitro*. *J. Physiol.-London*, **557**, 175–190.
- Bishop, G.H. & O'Leary, J.L. (1950) The effects of polarizing currents on cell potentials and their significance in the interpretation of central nervous system activity. *Electroencephalogr. Clin. Neurophysiol.*, **2**, 401–416.
- Briggman, K.L. & Denk, W. (2006) Towards neural circuit reconstruction with volume electron microscopy techniques. *Curr. Opin. Neurobiol.*, **16**, 562–570.
- Bullock, T.H. (1997) Signals and signs in the nervous system: The dynamic anatomy of electrical activity is probably information-rich. *Proc. Nat. Acad. Sci. USA*, **94**, 1–6.
- Chalmers, D.J. (2000) What is a neural correlate of consciousness? In: T. Metzinger, ed. *Neural Correlates of Consciousness: Empirical and Conceptual Questions*. MIT Press.
- Chen, K.C. & Nicholson, C. (2000) Spatial buffering of potassium ions in brain extracellular space. *Biophys. J.*, **78**, 2776–2797.
- Clark, J. & Plonsey, R. (1966) A mathematical evaluation of the core conductor model. *Biophys. J.*, **6**, 95.
- Clark, J. & Plonsey, R. (1968) Extracellular potential field of single active nerve fiber in a volume conductor. *Biophys. J.*, **8**, 842.

- Craig, D.P. & Thirunamachandran, T. (1984) *Molecular Quantum Electrodynamics: An Introduction to Radiation-Molecule Interactions*. London; Orlando: Academic Press.
- da Silva, F.H.L. & Van Rotterdam, AB (2005) Biophysical aspects of EEG and magnetoencephalogram generation. In: E. Niedermeyer and F.H.L. da Silva, eds. *Electroencephalography: Basic Principles, Clinical Applications, and Related Fields*. Philadelphia: Lippincott Williams & Wilkins, p. xiii.
- Dayan, P. & Abbott, L.F. (2001) *Theoretical Neuroscience: Computational and Mathematical Modeling of Neural Systems*. Cambridge, Mass.; London: MIT Press.
- de Graaf, T.A., Hsieh, P.-J. & Sack, A.T. (2012) The 'correlates' in neural correlates of consciousness. *Neurosci. Biobehav. Rev.*, **36**, 191–197.
- Destexhe, A. & Bedard, C. (2012) Do neurons generate monopolar current sources? *J. Neurophysiol.*, **108**, 953–955.
- Dilger, J.P., McLaughlin, S.G., McIntosh, T.J. & Simon, S.A. (1979) The dielectric constant of phospholipid bilayers and the permeability of membranes to ions. *Science*, **206**, 1196–1198.
- Einevoll, G.T., Kayser, C., Logothetis, N.K. & Panzeri, S. (2013) Modelling and analysis of local field potentials for studying the function of cortical circuits. *Nat. Rev. Neurosci.*, **14**, 770–785.
- Faber, D.S. & Korn, H. (1989) Electrical-field effects — their relevance in central neural networks. *Physiol. Rev.*, **69**, 821–863.
- Francis, J.T., Gluckman, B.J. & Schiff, S.J. (2003) Sensitivity of neurons to weak electric fields. *J. Neurosci.*, **23**, 7255–7261.
- Freeman, A.J. (1975) *Mass Action in the Nervous System: Examination of the Neurophysiological Basis of Adaptive Behavior through the EEG*. New York: Academic Press.
- Frohlich, F. & McCormick, D.A. (2010) Endogenous electric fields may guide neocortical network activity. *Neuron*, **67**, 129–143.
- Geddes, L.A. & Baker, L.E. (1967) Specific resistance of biological material—a compendium of data for biomedical engineer and physiologist. *Med. Biol. Eng.*, **5**, 271.
- Gold, C., Henze, D.A. & Koch, C. (2007) Using extracellular action potential recordings to constrain compartmental models. *J. Comput. Neurosci.*, **23**, 39–58.
- Gold, C., Henze, D.A., Koch, C. & Buzsaki, G. (2006) On the origin of the extracellular action potential waveform: A modeling study. *J. Neurophysiol.*, **95**, 3113–3128.
- Gold, C., Girardin, C.C., Martin, K.A.C. & Koch, C. (2009) High-amplitude positive spikes recorded extracellularly in cat visual cortex. *J. Neurophysiol.*, **102**, 3340–3351.
- Hagan, S., Hameroff, S.R. & Tuszynski, J.A. (2002) Quantum computation in brain microtubules: Decoherence and biological feasibility. *Phys. Rev. E*, **65**, 1–11.
- Hameroff, S. (1998) Quantum computation in brain microtubules? The Penrose-Hameroff 'Orch OR' model of consciousness. *Philos. Trans. R. Soc. London S. A-Math. Phys. Eng. Sci.*, **356**, 1869–1896.
- Hameroff, S. (2012) Quantum brain biology complements neuronal assembly approaches to consciousness: Comment on "Consciousness, biology and quantum hypotheses" by Baars and Edelman. *Phys. Life Rev.*, **9**, 303–305.
- Hameroff, S. & Penrose, R. (2013) Consciousness in the universe: A review of the 'Orch OR' theory. *Phys. Life Rev.*
- Hille, B. (2001) *Ion Channels of Excitable Membranes*. Sunderland, MA.: Sinauer Associates, Inc.

- Hines, M.L. & Carnevale, N.T. (1997) The NEURON simulation environment. *Neural Comput.*, **9**, 1179–1209.
- Hodgkin, A.L. & Huxley, A.F. (1952a) The components of membrane conductance in the giant axon of loligo. *J. Phys.-London*, **116**, 473–496.
- Hodgkin, A.L. & Huxley, A.F. (1952b) Currents carried by sodium and potassium ions through the membrane of the giant axon of loligo. *J. Physiol.-London*, **116**, 449–472.
- Hodgkin, A.L. & Huxley, A.F. (1952c) The dual effect of membrane potential on sodium conductance in the giant axon of loligo. *J. Physiol.-London*, **116**, 497–506.
- Hodgkin, A.L. & Huxley, A.F. (1952d) Propagation of electrical signals along giant nerve fibres. *Proc. R. Soc. London. Ser. B, Biol. Sci.*, **140**, 177–183.
- Hodgkin, A.L. & Huxley, A.F. (1952) A quantitative description of membrane current and its application to conduction and excitation in nerve. *J. Physiol.-London*, **117**, 500–544.
- Hodgkin, A.L., Huxley, A.F. & Katz, B. (1952) Measurement of current-voltage relations in the membrane of the giant axon of loligo. *J. Physiol.-London*, **116**, 424–448.
- Hohwy, J. (2012) Neural correlates and causal mechanisms. *Conscious. Cogn.*, **21**, 691–692.
- Holt, G.R. & Koch, C. (1999) Electrical interactions via the extracellular potential near cell bodies. *J. Comput. Neurosci.*, **6**, 169–184.
- Huang, W. & Levitt, D.G. (1977) Theoretical calculation of dielectric-constant of a bilayer membrane. *Biophys. J.*, **17**, 111–128.
- Izhikevich, E.M. (2007) *Dynamical Systems in Neuroscience: The Geometry of Excitability and Bursting*. Cambridge, Mass.; London: MIT Press.
- Jackson, J.D. (1999) *Classical Electrodynamics*. New York: Wiley.
- Jefferys, J.G.R. (1981) Influence of electric-fields on the excitability of granule cells in guinea-pig hippocampal slices. *J. Phys.-London*, **319**, 143–152.
- Jefferys, J.G.R. (1995) Nonsynaptic modulation of neuronal-activity in the brain — electric currents and extracellular ions. *Physiol. Rev.*, **75**, 689–723.
- Jefferys, J.G.R. & Haas, H.L. (1982) Synchronized bursting of CA1 hippocampal pyramidal cells in the absence of synaptic transmission. *Nature*, **300**, 448–450.
- John, E.R. (2001) A field theory of consciousness. *Conscious. Cognit.*, **10**, 184–213.
- John, E.R. (2002) The neurophysics of consciousness. *Brain Res. Rev.*, **39**, 1–28.
- John, E.R. (2003) A theory of consciousness. *Curr. Dir. Psychol. Sci.*, **12**, 244–250.
- John, E.R. (2005) From synchronous neuronal discharges to subjective awareness? *Progr. Brain Res.*, **150**, 143–593.
- John, E.R. (2006) The sometimes pernicious role of theory in science. *Int. J. Psychophysiol.*, **62**, 377–383.
- Johnston, D. & Wu, S.M.-S. (1995) *Foundations of Cellular Neurophysiology*. Cambridge, Mass.: MIT Press.
- Kandel, E.R. & Schwartz, J.H. (2000) *Principles of Neural Science*. New York: McGraw-Hill.
- Katz, B. (1966) *Nerve, Muscle, and Synapse*. New York: McGraw-Hill.
- Kinney, J.P., Spacek, J., Bartol, T.M., Bajaj, C.L., Harris, K.M. & Sejnowski, T.J. (2013) Extracellular sheets and tunnels modulate glutamate diffusion in hippocampal neuropil. *J. Comp. Neurol.*, **521**, 448–464.
- Köhler, W. (1960) *Dynamics in Psychology*. WW Norton & Company.
- Kuffler, S.W. & Nicholls, J.G. (1976) *From Neuron to Brain: A Cellular Approach to the Function of the Nervous System*. Sunderland, Mass.: Sinauer Associates.

- Lee, K.Y.C., Klingler, J.F. & McConnell, H.M. (1994) Electric-field-induced concentration gradients in lipid monolayers. *Science*, **263**, 655–658.
- Libet, B. (1994) A testable field theory of mind-brain interaction. *J. Conscious. Stud.*, **1**, 119–126.
- Libet, B. (1996) Conscious mind as a field. *J. Theor. Biol.*, **178**, 223–224.
- Lindahl, B.I.B. & Arhem, P. (1994) Mind as a force-field — comments on a new interactionistic hypothesis. *J. Theor. Biol.*, **171**, 111–122.
- Maggio, B., Borioli, G.A., Del Boca, M., De Tullio, L., Fanani, M.L., Oliveira, R. G., Rosetti, C.M. & Wilke, N. (2008) Composition-driven surface domain structuring mediated by sphingolipids and membrane-active proteins. *Cell Biochem. Biophys.*, **50**, 79–109.
- Magistretti, P.J. & Ransom, B.R. (2002) Chapter 10: Astrocytes. In: K.L. Davis, D. Charney, J.T. Coyle and C. Nemeroff eds. *Neuropsychopharmacology: The Fifth Generation of Progress*. Lippincott Williams & Wilkins.
- Malmivuo, J. & Plonsey, R. (1995) *Bioelectromagnetism: Principles and Applications of Bioelectric and Biomagnetic Fields*. New York: Oxford University Press.
- McFadden, J. (2002a) The conscious electromagnetic information (CEMI) field theory. *J. Conscious. Stud.*, **9**, 45–60.
- McFadden, J. (2002b) Synchronous firing and its influence on the brain's electromagnetic field: Evidence for an electromagnetic theory of consciousness. *J. Conscious. Stud.*, **9**, 23–50.
- McFadden, J. (2006) The CEMI field theory: Seven clues to the nature of consciousness. In: J. A. Tuszynski, ed. *The Emerging Physics of Consciousness*. Berlin Heidelberg: Springer, pp. 385–404.
- McFadden, J. (2013) The CEMI field theory closing the loop. *J. Conscious. Stud.*, **20**, 1–2.
- McIntyre, C.C. & Grill, W.M. (1999) Excitation of central nervous system neurons by nonuniform electric fields. *Biophys. J.*, **76**, 878–888.
- Metzinger, T. (2000) *Neural Correlates of Consciousness — Empirical and Conceptual Questions*. Cambridge MA: MIT Press.
- Mishchenko, Y., Hu, T., Spacek, J., Mendenhall, J., Harris, K.M. & Chklovskii, D.B. (2010) Ultrastructural analysis of hippocampal neuropil from the connectomics perspective. *Neuron*, **67**, 1009–1020.
- Molyneux, B. (2010) Why the neural correlates of consciousness cannot be found. *J. Conscious. Stud.*, **17**, 168–188.
- Mormann, F. & Koch, C. (2007) Neural correlates of consciousness. *Scholarpedia*, **2**, 1740.
- Neisser, J. (2012) Neural correlates of consciousness reconsidered. *Conscious. Cogn.*, **21**, 681–690.
- Nicholson, C. & Phillips, J.M. (1981) Ion diffusion modified by tortuosity and volume fraction in the extracellular micro-environment of the rat cerebellum. *J. Physiol.-London*, **321**, 225–257.
- Nicholson, C. & Sykova, E. (1998) Extracellular space structure revealed by diffusion analysis. *Trend. Neurosci.*, **21**, 207–215.
- Noebels, J.L. & Prince, D.A. (1978) Excitability changes in thalamocortical relay neurons during synchronous discharges in cat neocortex. *J. Neurophys.*, **41**, 1282–1296.
- Nunez, P.L. & Srinivasan, R. (2006) *Electric Fields of the Brain: The Neurophysics of EEG*. Oxford, New York: Oxford University Press.
- Parra, L.C. & Bikson, M. (2004) Model of the effect of extracellular fields on spike time coherence. *Proc. 26th Ann. Int. Conf. IEEE Eng. Med. Biol. Soc.*, 1–7. 4584–4587.

- Peterka, D.S., Takahashi, H. & Yuste, R. (2011) Imaging voltage in neurons. *Neuron*, **69**, 9–21.
- Pethig, R. (1986) Ion, electron, and proton transport in membranes: A review of the physical processes involved. In: F. Gutmann and H. Keyzer eds. *Modern Bioelectrochemistry*. New York: Plenum Press, pp. 199–239.
- Plonsey, R. (1964) Volume conductor fields of action currents. *Biophys. J.*, **4**, 317.
- Plonsey, R. & Collin, R. (1961): *Principles and Applications of Electromagnetic Fields*. New York: McGraw Hill.
- Plonsey, R. & Heppner, D.B. (1967) Considerations of quasi-stationarity in electrophysiological systems. *Bull. Math. Biophys.*, **29**, 657.
- Plonsey, R. & Fleming, D.G. (1969) *Bioelectric Phenomena*. New York: McGraw-Hill.
- Pockett, S. (1999) Anesthesia and the electrophysiology of auditory consciousness. *Conscious. Cognit.*, **8**, 45–61.
- Pockett, S. (2000) *The Nature of Consciousness: A Hypothesis*. Writer's Club Press.
- Pockett, S. (2002) Difficulties with the electromagnetic field theory of consciousness. *J. Conscious. Stud.*, **9**, 51–56.
- Pockett, S. (2007) Difficulties with the electromagnetic field theory of consciousness: An update. *NeuroQuantology*, **3**, 271–275.
- Pockett, S. (2012) The electromagnetic field theory of consciousness a testable hypothesis about the characteristics of conscious as opposed to non-conscious fields. *J. Conscious. Stud.*, **19**, 191–223.
- Popper, K.R., Lindahl, B.I.B. & Arhem, P. (1993) A discussion of the mind-brain problem. *Theor. Med.*, **14**, 167–180.
- Poznanski, R.R. & Cacha, L.A. (2012) Intracellular capacitive effects of polarized proteins in dendrites. *J. Integr. Neurosci.*, **11**, 417–437.
- Rall, W. & Shepherd, G.M. (1968) Theoretical reconstruction of field potentials and dendrodendritic synaptic interactions in olfactory bulb. *J. Neurophys.*, **31**, 884.
- Reato, D., Rahman, A., Bikson, M. & Parra, L.C. (2010) Low-intensity electrical stimulation affects network dynamics by modulating population rate and spike timing. *J. Neurosci.*, **30**, 15067–15079.
- Reimann, M.W., Anastassiou, C.A., Perin, R., Hill, S.L., Markram, H. & Koch, C. (2013) A biophysically detailed model of neocortical local field potentials predicts the critical role of active membrane currents. *Neuron*, **79**, 375–390.
- Romijn, H. (2002) Are virtual photons the elementary carriers of consciousness? *J. Conscious. Stud.*, **9**, 61–81.
- Sadiku, M.N.O. (2001) *Elements of Electromagnetics*. New York: Oxford University Press.
- Shanahan, M. & Baars, B. (2005) Applying global workspace theory to the frame problem. *Cognition*, **98**, 157–176.
- Speckmann, E.-J. & Elgar, C.E. (2005) Introduction to the neurophysiological basis of the EEG and DC potentials. In E. Niedermeyer and F. H. Lopes da Silva eds. *Electroencephalography: Basic Principles, Clinical Applications, and Related Fields*, Philadelphia: Lippincott Williams & Wilkins, pp. 17–29.
- Sykova, E. (1997) The extracellular space in the CNS: Its regulation, volume and geometry in normal and pathological neuronal function. *Neuroscientist*, **3**, 28–41.
- Sykova, E. (2004) Extrasynaptic volume transmission and diffusion parameters of the extracellular space. *Neuroscience*, **129**, 861–876.

- Sykova, E. & Nicholson, C. (2008) Diffusion in brain extracellular space. *Physiol. Rev.*, **88**, 1277–1340.
- Sykova, E., Roitbak, T., Mazel, T., Simonova, Z. & Harvey, A.R. (1999) Astrocytes, oligodendroglia, extracellular space volume and geometry in rat fetal brain grafts. *Neuroscience*, **91**, 783–798.
- Taylor, C.P. & Dudek, F.E. (1982) Synchronous neural after discharges in rat hippocampal slices without active-chemical synapses. *Science*, **218**, 810–812.
- Terzuolo, C.A. & Bullock, T.H. (1956) Measurement of imposed voltage gradient adequate to modulate neuronal firing. *Proc. Nat. Acad. Sci. USA*, **42**, 687–694.
- Tononi, G. (2008) Consciousness as integrated information: A provisional manifesto. *Biol. Bull.*, **215**, 216–242.
- Tononi, G. (2004) An information integration theory of consciousness. *BMC Neurosci.*, **42**.
- Van Harrenveld, A. (1968) The extracellular space in the vertebrate central nervous system. In: G.H. Bourne, ed. *The Structure and Function of Nervous Tissue*. New York: Academic Press, pp. 447–511.
- Velmans, M. & Schneider, S. eds. (2007) *The Blackwell Companion to Consciousness*. Malden, MA; Oxford: Blackwell Publishing.
- Weiss, S.A. & Faber, D.S. (2010) Field effects in the CNS play functional roles. *Front. Neural Circuits*, **4**.